3. THE PRINCIPAL CLIMATIC PARAMETERS

The principal climatic parameters at any given meteorological station are the potential inflow of solar radiation and the characteristics of the surrounding, so-called "active surface". The inflow of solar energy (insolation) depends on latitude, which determines the peak height of the Sun and duration of day and night, deciding the potential duration of the insolation and its seasonal differentiation. The Polish Polar Station is located on the northern shore of the wide mouth of Hornsund Fjord on the SW coast of Spitsbergen. The island is a relatively small land area surrounded by the ocean. This means that the basic type of surface surrounding station and island is an open water surface. In contrast to stable land surroundings (neglecting the seasonal occurrence of snow cover), the surface water surrounding SW Spitsbergen is characterized by strong and large scale changes of ocean surface temperature and the character and extent of ice cover.

3.1. Duration of day and night

The Hornsund station is located at Latitude 77°N. This causes strong differences in the duration of day and night. The Sun is seen at the station for 261 days, between February 12 and October 30. From October 31 to February 11 the Sun is below horizon, giving a polar night that lasts 104 days. From the moment of the Sun's appearance above the horizon (February 12) daylight increases rapidly and on April 24 full polar day begins that continues to August 18 (117 days). At Hornsund the duration of polar day and polar night are for 11 days shorter than at the Ny Ålesund station situated in the northern part of Spitsbergen. In the region of the Polish Polar Station the Sun reaches maximum height (h_s) on June 22, when at midday it is 36°23.7' above the horizon. From August 19 Sun is again rising and setting while day is getting shorter very quickly. The phenomenon of white nights ($-6° \leq h_S \leq -0°50'$) is observed on April 7– 23 and on August 19 – September 6. Distribution of Sun altitude and timing of dawn and twilight appearance (civil: $-6° \leq h_S \leq -0°50'$, nautical: $-12° \leq h_S < -6°$ and astronomical: $-18° \leq h_S < -12°$) are shown on Fig. 3.1.

There are big changes in the duration of the day at the Hornsund station during the year. The register of sunrise and sunset timing is given in Table 3.1. These data are for the mean solar time of the station. Timing of sunrise and sunset are calculated according to the intersection (covering) half of the Sun's disk by the horizon, taking into consideration effects of astronomical refraction (34'); in the calculations the radius of the Sun and cloud covering of the horizon were not taken into account. Accuracy of calculations of timing of sunrises and sunsets is ±0.75 minute and is corrected with an established algorithm for rounding times of sunrise and sunset.

Duration of the day calculated on the basis of values given in Table 3.1 is identical with absolute insolation (astronomical), and duration of sun corresponds to the so-called maximum possible insolation (SSa) and does not take into consideration any cloud covering of the horizon. Annual total of insolation SSa amounts to 4552.95 hours and monthly totals range from 81.95 hours in February to 744.0 hours in May and July when there is full polar day. Distribution of monthly total

SSa and minimum and maximum daily totals are given in Table 3.2. If the horizon at the survey point is not anywhere covered, a full 24 hours of diurnal insolation is theoretically possible during a polar day. However, such a duration of insolation is never possible at the Hornsund station because in both the near and distant surroundings there are obstructions (hills) of different heights.

Table 3.1. Timing of astronomic sunrise (SA) and sunset (SU) [mean solar time; hours and minutes] at φ = 77°N.

Day	February		March		April		August		September		October	
	SA	SU	SA	SU	SA	SU	SA	SU	SA	SU	SA	SU
1			08 06	15 54	04 27	19 33			03 09	20 51	06 45	1715
2			07 59	16 02	04 20	19 41			03 18	20 42	06 51	1709
3			07 51	16 09	04 12	19 48			03 26	20 35	06 59	1702
4			07 44	16 17	04 05	19 56			03 35	20 26	07 06	1654
5			07 36	16 24	03 57	20 03			03 42	20 18	07 12	1648
6			07 28	16 32	03 48	20 12			03 50	20 11	07 20	1641
7			07 21	16 39	03 41	20 20			03 59	20 02	07 27	1633
8			07 14	16 47	03 33	20 27			04 06	19 54	07 35	1626
9			07 08	16 53	03 24	20 36			04 14	19 47	07 41	1620
10			07 00	17 00	03 15	20 45			04 21	19 39	07 48	1612
11			06 53	17 08	03 08	20 53			04 27	19 33	07 56	1605
12	11 51	12 09	06 45	17 15	02 57	21 03			04 35	19 26	08 05	1556
13	11 06	12 54	06 39	17 21	02 48	21 12			04 42	19 18	08 12	1548
14	10 45	13 15	06 32	17 29	02 39	21 21			04 50	19 11	08 20	1541
15	10 27	13 33	06 26	17 35	02 29	21 32			04 56	19 05	08 27	1533
16	10 12	13 48	06 18	17 42	02 17	21 44			05 03	18 57	08 36	1524
17	10 00	14 00	06 11	17 50	02 06	21 54			05 09	18 51	08 45	1515
18	09 48	14 12	06 05	17 56	01 53	22 08			05 17	18 44	08 53	1508
19	09 36	14 24	05 57	18 03	01 39	22 21	00 08	23 52	05 24	18 36	09 02	1459
20	09 25	14 35	05 51	18 09	01 23	22 35	00 12	23 33	05 30	18 30	09 12	1448
21	09 15	14 45	05 44	18 17	01 03	22 57	00 47	23 13	05 38	18 23	09 21	1439
22	09 06	14 54	05 38	18 23	00 32	23 29	01 11	22 50	05 44	18 17	09 32	1429
23	08 57	15 03	05 30	18 30	00 01	23 59	01 29	22 32	05 51	18 09	09 42	1418
24	08 48	15 12	05 23	18 38			01 44	22 17	05 57	18 03	09 54	1406
25	08 39	15 21	05 17	18 44			01 57	22 03	06 05	17 56	10 06	1354
26	08 30	15 30	05 09	18 51			02 09	21 51	06 11	17 50	10 20	1341
27	08 23	15 28	05 03	18 57			02 21	21 39	06 18	17 42	10 36	1324
28	08 14	15 47	04 56	19 05			02 32	21 29	06 24	17 36	10 54	1306
29	-	-	04 48	19 12			02 42	21 18	06 32	17 29	11 21	1239
30	-	-	04 41	19 20			02 51	21 09	06 38	17 23	11 52	1209
31	-	-	04 35	19 26			03 00	21 00	-	-	Polar night	

Polar night: 1 – 10
Polar day: 19 – 31
Polar day: 1 – 18
Polar day: 24 – 30

The physical horizon observed from the survey site in the meteorological plot was determined by theodolite measurements in July 2003 (Fig. 3.2). The surroundings of the station have a varied relief. Altitudes and general orientation of particular landforms create distinct preferential inflows of radiant energy to the ground surface in the station surroundings before and at noon. The biggest inflow is from hills with the height more than 500 m a.s.l. nearest to the station. To the north these are the Ariekammen – Fugleberget range with a culmination at 568.7 m a.s.l. and, further to the NW, Skoddefjellet (733 m a.s.l.) which lies on a bearing close to the SW ridge of Ariekammen. Horizon cover in the azimuth range 320–022° exceeds 10°, reaching a maximum of 14.2° at 016°.

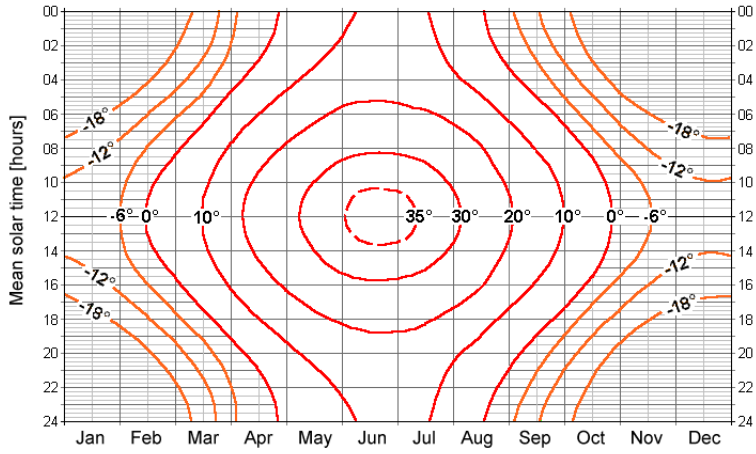

Fig. 3.1. Isopleth diagram of the solar altitude. Civil (h_S = –6°), nautical (h_S = –12°) and astronomical (h_S = –18°) twilight. Dashed field – Sun below the horizon.

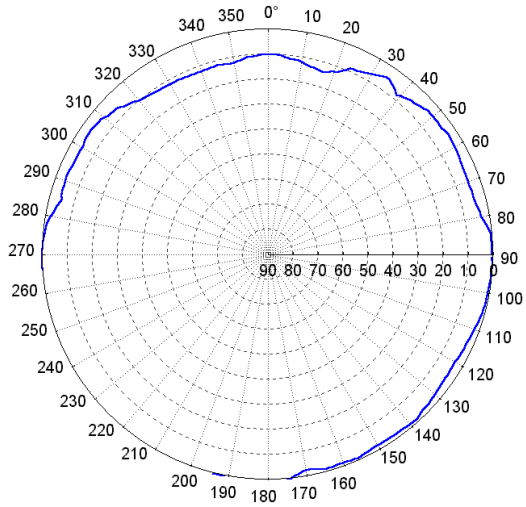

Fig. 3.2. Topographic obstruction effects along the horizon at the Hornsund station (as in July 2003).

On June 22 at the midnight the solar angle is 10.5°. Obstructions shut it out half an hour later when the Sun reaches an angle of 11.4° at azimuth 021°. At the end of this day (at 22:06 of mean solar time) the Sun is hidden behind the SW part of Ariekammen when it is at 334° azimuth and an angle of 11.9°.

The duration of direct sunlight as determined by the astronomical timing of sunrise and sunset plus obstruction of the horizon by natural heights defines "possible insolation" (SSp). Duration of insolation measured is additionally limited by the precision of the instruments. The basic meteorological instrument used for measurements of insolation is heliograph. At the Hornsund station measurements

of insolation are done with two Campbell-Stokes heliographs, which start recording direct solar radiation at a solar altitude (angle) of 3°. This may take place between March 24 and October 19. The distribution of monthly totals and minimum and maximum daily totals of possible insolation (SSp) with obstructions of the horizon as well as precision of instruments taken into consideration is shown in Table 3.2. The annual total of possible insolation amounts to 3541.8 hours and changes from 14.8 hours in February to more than 600 hours in June and July. In June for 15 days (June 16–30) duration of potential insolation may be 20.5 hours.

Table 3.2. Monthly totals, maximum (max) and minimum (min) daily astronomical insolation (SSa) and possible insolation (SSp) within the month [hours] and relative possible insolation (r.SS = SSp/SSa; %) at Hornsund.

	Jan	Feb	March	April	May	June	July	Aug	Sept	Oct	Nov	Dec
SSa	-	82.0	352.7	592.9	744.0	720.0	744.0	698.6	422.6	196.3	-	-
min	-	0.3	7.8	15.1	24.0	24.0	24.0	18.0	10.8	0.0	-	-
max	-	7.6	14.9	24.0	24.0	24.0	24.0	24.0	17.4	10.5	-	-
SSp	-	14.8	271.4	452.6	588.3	609.5	612.6	533.5	353.3	105.8	-	-
min	-	0.0	4.4	12.7	17.6	19.9	19.1	14.4	8.3	0.0	-	-
max	-	4.1	12.5	17.5	19.9	20.5	20.4	19.1	14.3	8.1	-	-
r.SS	-	18.0	76.9	76.3	79.1	84.7	82.3	76.4	83.6	53.9	-	-

The influence of local hypsometric conditions on the duration of insolation expresses potential relative insolation (r.SS) relative to absolute insolation. From the calculations shown in Table 3.2, monthly totals of possible insolation at the Hornsund station range from 18% in February to 84.7% in June. Over the course of the year topographic obstacles and precision of instruments reduce the duration of potential insolation by 22.2%. More than half (51.1%) of the annual total of possible insolation may occur in the three months of continuous polar day (May-July). High total of monthly potential insolation was calculated also for August (533.5 hours), in first twenty days of which polar day conditions continue.

3.2. Potential insolation

Inflow of radiant solar energy is one of the most important factors determining atmospheric conditions. It also limits a number of the biotic and abiotic processes acting in the environment. Monthly totals of potential total radiation (i.e. radiation maximally possible if there is no cloud cover (R_Q) establish the possible inflow of solar radiation to horizontal surfaces in the Hornsund region. These values have been calculated with the method of A. Styszyńska (1995) with the computer program "POLEPODS". This program allows for determination of potential inflow of radiant solar energy with allowance for all astronomical factors and processes of reducing solar radiation in the atmosphere in relation to its transparency. A solar constant of 1367 $W \cdot m^{-2}$ (according to Commission for Instruments and Methods of Observation, WMO) was used for calculations of radiation at the upper boundary of the atmosphere (Io). Solar radiation passing through the atmosphere undergoes reduction. The magnitude of this reduction depends on the length of the path of sunrays in the atmosphere, defined by optical mass of the atmosphere. Calculations of optical mass of atmosphere

were done with an equation used by Bryazgin *et al*. (1983) when calculating the radiation regime of the Greenland and Norwegian Seas.

Other factors reducing solar radiation passing through the atmosphere are the concentrations of water vapour and particulates in the air. An index characterizing their contents in the air is a coefficient of transparency of the atmosphere (p_2). Review of the literature shows great spatial and temporal differentiation of p_2 values in the Arctic. In the region of southern Spitsbergen p_2 value may range from a mean of 0.78 in June and August, 0.79 in July and September, 0.81 in October to 0.82 in March, April and May (Bryazgin *et al*. 1983). In the Arctic transparency of the atmosphere depends on the water vapour content. The warmer the air the more humidity there is in it. Because air transparency varies between and within air masses, taking into account cyclonic activity (which is well developed in the region of southern Spitsbergen) it can be expected that p_2 value may display big fluctuations even over short periods. As a result, the hourly and daily potential radiation may have equally big fluctuations. The air masses most often present over Spitsbergen are characterized by overestimated transparency ($0.75 < p_2 < 0.80$) or high ($p_2 \geq 0.81$), momentarily reaching a transparency close to the ideal atmosphere ($p_2 = 0.88$). Bearing in mind the big differentiation of the transparency coefficient p_2 in southern Spitsbergen the total potential radiation reaching the ground surface at Hornsund was estimated to be in the range of the changes of the coefficient of atmosphere transparency, from 0.75 to 0.88. Monthly totals of total potential radiation for different values of p_2 coefficient are given in Table 3.3.

Table 3.3. Monthly totals of maximum possible total radiation at cloudless sky [MJ·m^{-2}] arriving to horizontal surface at φ = 77°N, at different values of p_2 and Io = 1367 W·m^{-2}.

p_2	February	March	April	May	June	July	August	September	October
0.75	0.155	41.795	227.257	506.989	651.918	599.824	344.828	101.257	5.379
0.76	0.186	44.717	237.014	524.311	672.189	619.247	357.939	106.823	5.952
0.77	0.221	47.823	247.108	542.092	692.904	639.136	371.446	112.649	6.581
0.78	0.263	51.126	257.550	560.346	714.071	659.501	385.364	118.747	7.274
0.79	0.313	54.637	268.354	579.087	735.700	680.355	399.705	125.129	8.035
0.80	0.372	58.369	279.531	598.330	757.798	701.709	414.486	131.809	8.872
0.81	0.441	62.338	291.098	618.091	780.374	723.574	429.722	138.799	9.792
0.82	0.522	66.557	303.068	638.386	803.438	745.964	445.433	146.116	10.804
0.83	0.619	71.045	315.458	659.234	826.998	768.891	461.636	153.775	11.918
0.84	0.732	75.818	328.287	680.653	851.064	792.368	478.352	161.793	13.143
0.85	0.866	80.897	341.572	702.663	875.646	816.410	495.604	170.188	14.491
0.86	1.024	86.302	355.336	725.284	900.753	841.029	513.414	178.979	15.977
0.87	1.210	92.056	369.599	748.539	926.395	866.242	531.810	188.188	17.614
0.88	1.429	98.185	384.387	772.450	952.582	892.062	550.820	197.837	19.419

A characteristic feature of monthly totals of potential total radiation is the great variability from month to month (Table 3.3). Annual total solar radiation at the upper border of the atmosphere amounts to 5939.611 MJ·m^{-2}, and annual totals R_Q that may reach the horizontal surface at the defined coefficient of atmosphere transparency range from 2479.402 MJ·m^{-2} at $p_2 = 0.75$ to 3869.171 MJ·m^{-2} at $p_2 = 0.88$. This amounts to 41.7 to 65.1% of incoming annual total radiation at the upper boundary of the atmosphere.

The highest inflow of radiant energy from the Sun can be during the continuous polar day when it reaches its highest elevation and the day lasts 24 hours. With the lack of cloudiness experienced in June-July around 50% of the annual total of R_Q (at p_2 = 0.75 – 46.7%, at p_2 = 0.88 – 47.7%) and from 21% (p_2 = 0.75) to 31% (p_2 = 0.88) of annual total radiation from the upper atmosphere may reach a given horizontal surface. Over the full period of polar day conditions (24 April – 18 August) the total OR that may reach horizontal surfaces in the Hornsund region is 2097.163 MJ·m^{-2} at p_2 = 0.75 and 2548.616 MJ·m^{-2} at p_2 = 0.82. This amounts to 84.6 to 80.6% of annual R_Q total, respectively. During the months of continuous polar day differences between monthly totals R_Q calculated for greatest q values are relatively small and do not exceed 33–37%. These differences suddenly grow bigger when the day is getting shorter, reaching 72% in October and as much as 89% in February.

Distribution of hourly total of potential solar radiation and its variability within a year are very big (Table 3.4). The highest hourly totals obviously may occur during the continuous polar day. On June 22 at midday (between 11:00 and 13:00 LT) hourly totals of potential solar radiation amount to 1.8544 MJ·m^{-2} at p_2 =0.78 and 2.0174 MJ·m^{-2} at p_2 =0.82. On this day at p_2 =0.78, for 12 hours (from 0600 to 1800 LT) hourly totals of potential total solar radiation can be higher than 1 MJ/m^2 (p_2 =0.28 for 14 hours). Values of R_Q exceeding 1 MJ/m^2 around midday can occur between April 12 and September 1. Such values of R_Q can occur on average for four hours during a day in April, 10 hours in May, 12 hours in June and July and 8 hours in August. During the lowest elevations of the Sun, hourly totals of R_Q do not exceed a few dozen J/m^2.

Table 3.4. Hourly totals of maximally possible total radiation at cloudless sky (R_Q) [MJ·m^{-2}] at φ = 77°N, in the middle day of month at p_2 = 0.82 and Io = 1367 W·m^{-2}.

Hour	February	March	April	May	June	July	August	September	October
00–01	-	-	-	0.0808	0.2977	0.2103	0.0013	-	-
01–02	-	-	-	0.1113	0.3464	0.2547	0.0061	-	-
02–03	-	-	0.0000	0.1878	0.4436	0.3456	0.0299	-	-
03–04	-	-	0.0030	0.3116	0.5888	0.4856	0.0999	-	-
04–05	-	-	0.0431	0.4835	0.7756	0.6686	0.2314	-	-
05–06	-	-	0.1612	0.6942	0.9931	0.8837	0.4155	0.0044	-
06–07	-	0.0001	0.3418	0.9241	1.2246	1.1141	0.6313	0.0598	-
07–08	-	0.0118	0.5475	1.1539	1.4519	1.3419	0.8538	0.1900	-
08–09	-	0.0755	0.7484	1.3640	1.6580	1.5494	1.0612	0.3514	0.0000
09–10	-	0.1742	0.9193	1.5380	1.8279	1.7195	1.2335	0.5016	0.0058
10–11	-	0.2614	1.0428	1.6607	1.9476	1.8403	1.3568	0.6142	0.0267
11–12	0.0000	0.3108	1.1059	1.7240	2.0090	1.9016	1.4194	0.6724	0.0459
12–13	0.0000	0.3108	1.1059	1.7240	2.0090	1.9016	1.4194	0.6724	0.0459
13–14	-	0.2614	1.0428	1.6607	1.9476	1.8403	1.3568	0.6142	0.0267
14–15	-	0.1742	0.9193	1.5380	1.8279	1.7195	1.2335	0.5016	0.0058
15–16	-	0.0755	0.7484	1.3640	1.6580	1.5494	1.0612	0.3514	0.0000
16–17	-	0.0118	0.5475	1.1539	1.4519	1.3419	0.8538	0.1900	-
17–18	-	0.0001	0.3418	0.9241	1.2246	1.1141	0.6313	0.0598	-
18–19	-	-	0.1612	0.6942	0.9931	0.8835	0.4154	0.0044	-
19–20	-	-	0.0431	0.4835	0.7756	0.6686	0.2314	-	-
20–21	-	-	0.0030	0.3116	0.5888	0.4856	0.0999	-	-
21–22	-	-	0.0000	0.1878	0.4436	0.3456	0.0299	-	-
22–23	-	-	-	0.1113	0.3464	0.2547	0.0061	-	-
23–24	-	-	-	0.0808	0.2977	0.2103	0.0013	up to	-

At solar angles in the northern quadrant, lower than 14°, eastern <5°, southern <3° and western <5° part of the possible inflow of potential solar radiation will be cut off by the mountainous relief. Around the meteorological site at the Hornsund station these losses are small during a short day and increase during the first period of continuous polar day.

In comparison with unobstructed areas, these amount up to 2% in March and August, up to 5% in February, July, September and October and up to 5–13% in other months, depending on the assumed coefficient of atmosphere transparency (Table 3.5).

Table 3.5. Monthly lowest (dmin) and highest (dmax) daily totals of maximum possible total radiation with cloudless sky [MJ·m^{-2}] reaching a horizontal surface (R_Q) with sheltering of the horizon ($c.R_Q$) taken into consideration at the Hornsund station, at different values of p_2 and Io = 1367 W·m^{-2} .

Element	February	March	April	May	June	July	August	September	October
p_2 = 0.75									
R_Q	0.155	41.795	227.257	506.989	651.918	599.824	344.828	101.257	5.379
$c.R_Q$	0.151	41.126	204.770	481.133	570.428	583.629	343.104	99.159	5.266
ΔR_Q	0.004	0.669	22487	25.856	81.490	16.195	1.724	1.001	0.113
% R_Q	97.4	98.4	90.1	94.9	87.5	97.3	99.5	98.9	97.9
R_Q dmin	0	0.0727	3.8111	12.0321	20.3077	15.8438	6.8175	0.9345	0
$c.R_Q$ dmin	0	0.0726	3.8108	12.0079	19.7148	15.5990	6.8067	0.9341	0
R_Q dmax	0.0527	3.5940	11.7288	20.1206	22.2495	21.8511	15.5558	6.5534	0.8299
$c.R_Q$ dmax	0.0526	3.5938	11.6991	19.2408	21.5771	21.1899	15.4456	6.5439	0.8032
p_2 = 0.82									
R_Q	0.522	66.557	303.068	638.386	803.438	745.964	445.433	146.116	10.804
$c.R_Q$	0.495	65.226	282.762	581.570	698.188	718.363	441.424	139.541	10.393
ΔR_Q	0.027	1.331	20.306	56.816	105.250	27.601	4.009	6.575	0.411
% R_Q	94.8	98.0	93.3	91.1	86.9	96.3	99.1	95.5	96.2
R_Q dmin	0	0.1982	5.4880	15.4694	25.1810	20.0113	9.1962	1.6274	0
$c.R_Q$ dmin	0	0.1979	5.4865	15.3747	24.1813	19.5033	9.1608	1.6269	0
R_Q dmax	0.1532	5.2117	15.1057	24.9687	27.3624	26.9140	19.6738	8.8747	1.4725
$c.R_Q$ dmax	0.1524	5.2107	15.0220	23.9842	26.2864	25.8393	19.4847	8.8437	1.4087

The greatest impact of relief on the magnitude of possible insolation is evident in June, when screening at the horizon cuts off 13% of the monthly total of potential radiation compared to unsheltered surfaces. From April to August inclusive these losses result first of all from the obstruction of the horizon in the northern quadrant by the Skoddefjellet and Ariekammen – Fugleberget mountain ranges.

The varying morphology in the vicinity of the station will lead to further spatial variation in insolation reaching the surfaces of particular landforms. The level of such differentiation will depend on exposure of an area and its inclination. On that score clearly privileged will be those slopes of the Ariekammen – Fugleberget range having sufficient southern exposure. The southern slopes of this range, with inclinations around 32° can receive nine times more energy than horizontal surfaces in February. In other months this effect is smaller, 3.1 in March, 1.8 in April, during continuous polar day it reduces to 1.1–1.3, increasing again during the autumn: 2.4 in September and 4.8 in October.

Given favourable conditions when the insolation may be very high, there will be significant differences in the warming of particular areas of the surface, leading to changes in the heat balance of these surfaces and resulting changes of temperature in the layer of air close to the ground. The further consequence of such situations can be development of local convection cells and changes in the cloud cover connected with them. As a result radiation-dominated weather characteristic of summer may develop. Such type of weather can occur especially when there is no wind or winds are weak.

Great changes in the amount of insolation, both temporal and spatial, occurring within relatively small areas will lead to considerable differentiation of micro- and topo- climatic conditions. It will also influence formation of other features of the environment of this region (e.g. processes of freezing and thawing of the ground, occurrence of polygonal soils, processes of frost disintegration, rates of ablation etc.).

3.3. Changes in the sea ice area and the surface temperatures of surrounding seas

Spitsbergen is surrounded by seas (Fig. 2.1). Its western coast is washed by the Greenland Sea, northern by the Arctic Ocean. The eastern coast of Spitsbergen is washed by the Barents Sea and at the southern end (Sörkapp Land) is the northernmost part of the Norwegian Sea (Limits of Oceans and Seas, 1953).

Changes of the surface state of these vast bodies of water exert influences on the climatic features of Spitsbergen, including Hornsund. This influence is very strong because the area of the archipelago is negligibly small in relation to the area of surrounding seas.

The most important features of the surrounding seas that influence the climate of Spitsbergen are interrelated sea surface temperature (SST) and sea ice cover (SIC). Both SST and SIC show changeability within a year and between years. Both types of changeability are reflected in the variability of the Hornsund climate.

SST influences flow of heat and humidity from the ocean to the atmosphere and the rates of transformation of air masses flowing over the water. In every case where the air flowing over water is colder processes of convection develop both in the ocean and in atmosphere. Surface water cooled by the heat loss increases its density and sinks ("goes under"), and in its place warmer water rises to the surface. Heat taken from the ocean surface warms the air, creating a deficit in humidity. This enhances evaporation from the ocean surface. The density of this heated air is decreasing and forces of hydrostatic lift begin – ascending currents develop, transporting open and latent heat (together with water vapour) to the higher layers of the troposphere, inducing compensatory down flows of cooler air. As a result differences of temperature between water and air persist, allowing long-lasting convection.

The intensity of heat flow from the ocean to the atmosphere is directly proportional to the difference of temperature between water and air (ΔT), difference between maximum pressure at the temperature of the sea surface and actual pressure in the air above the water (Δe), and wind velocity over the water (Vw). The greater the wind velocity and higher are Δt and Δe, the higher are the flows of open and latent heat and thus the flux of water vapour. In the Arctic conditions

prevailing around Spitsbergen the intensity of heat fluxes may reach very big values[1], contributing to very rapid increases of air temperature and of water vapour in the air.

In the event of inflow of air warmer than the water any flux of heat from the ocean to the atmosphere ceases and the temperature of the closest air layer decreases to that of the water surface[2]. This produces an inversion of temperature in the air above the water (= extremely stable equilibrium) and the exchange of heat between the atmosphere and the ocean surface ceases. Simultaneously there is an increase in the coefficient of friction velocity and the gustiness of the wind over the water decreases.

These transformations occur at different rates. When the temperature of the inflowing air is lower than the water temperature the transformation is very fast and extends to upper reaches of the convection. When the temperature of air is higher than the water adjustment occurs slowly, with stronger changes only affecting the lower air.

When there is sea ice cover because of its weak thermal conductivity it cuts off any heat flow from the ocean to the atmosphere. Heat flow through ice becomes two-three orders of magnitude smaller[3] than heat flow from the water surface. In such conditions transformation of air cooler than the ice surface becomes very slow – the rates of radiative cooling significantly exceed heat flow through the ice. This creates favourable conditions for strong cooling of the air above the SIC, especially when there is a lack of insolation (formation of Arctic – continental air masses) and the creation of deep inversions (Chase *et al.* 2002).

Sea ice cover may be formed in conditions when heat flow from the ocean to the atmosphere becomes bigger than any heat flow to the sea surface by convection within the water[4], and water temperature will reach freezing point. Deficiency of heat in the surface water layer is then compensated by the latent heat of crystallization. After the formation of ice heat flux from the ocean to the atmosphere undergoes sudden limitation. Covering a body of water with sea ice may also occur without connection with its transient heat balance, under the influence of dynamic factors – when ice drifts into the given body of water from elsewhere under the influence of wind, wind-driven current or current alone.

---

1 Equations for calculations of heat transfer from the ocean to the atmosphere are not reported here. For example, at SST equal 0°C, temperature of air flowing above water equal –5°C, its actual pressure e = 3,0 hPa (relative humidity ~72%) and wind velocity above water equal 10 m/s, calculated with appropriate equations losses of heat from the sea surface amount 20.74 $MJ \cdot m^{-2}$ during the day (including losses of heat for turbulence exchange 10.60 $MJ \cdot m^{-2}$ for a day, losses of heat for evaporation 10.14 $MJ \cdot m^{-2}$ for a day). For the same parameters for air and wind, but a water surface temperature of +3°C, losses of heat from 1 m^2 of sea surface amount to 31.49 MJ per day.

2 In non-stratified waters temperature of water in the vertical profile is the highest on the surface (thus density of water is the lowest), strong hydrostatic stability occurs in water (equivalent of extremely stable equilibrium in the atmosphere), excluding convection. Δt on the water-air boundary becomes equal to zero, relative humidity is 100%. As a result, the exchange of open heat as well as heat of evaporation is least (the flux of water vapour becomes zero).

3 Depending on the thickness of sea ice and extent of its cover. At a cover of ice of 7 and more (70% of water surface covered with ice), differences in the size of heat fluxes between total cover (10) and such density (7) become negligibly small.

4 Duration of convection processes depends in turn on the amount of heat in waters. This in essence depends on the thermohaline structure of the waters. The bigger resources of heat, the longer duration of convection.

Over the course of SSTand SIC changes in the water surrounding Spitsbergen clear seasonal change is evident, associated with the behaviour of the radiation and heat balance variables within a given year. However, processes of water circulation and atmospheric circulation decide inter-seasonal and inter-annual variability in the spatial distribution of SST and SIC in these bodies of water.

3.3.1. Sea surface temperature

Along the western coast of Spitsbergen the warm West Spitsbergen Current (WSC) flows to the north, as a strip around 50 NM wide approximately parallel to the continental slope outside of the lower edge of the Spitsbergen shelf. It carries warm Atlantic water (5–7°C) of high salinity (35.1–35.3 PSU; Aagard *et al.* 1987, Piechura *et al.* 2001). Periodically warm water of the WSC flows onto the Spitsbergen shelf. The Atlantic water does not show thermohaline stratification[5],its heat resources are very big, greater than can possibly be exhausted during the winter even if the latter is significantly stronger than average. To the west of the WSC axis in the open water of the Greenland Sea, SST is clearly lower but salinity decreases only very slightly and convection may extend to great depths. At the NW end of Spitsbergen this water divides. Part of it flows further north and through Fram Strait into the Arctic Sea basin, "sinking" under the ice and Arctic Surface Water (ASW) with its lower density. Part flows eastwards and then NE, passing around the northern coast of Spitsbergen and Nordaustlandet. Here, as water of higher salinity it sinks under the cooler ASW. Part of the WSC water in Fram Strait, turns back southwards. Thanks to the warming activity of the WSC, the water west of Spitsbergen is the northernmost body of water free of ice on the Earth (Haugan 1999).

On the eastern side of Spitsbergen, in the NW sector of the Barents Sea, strongly cooled and desalted Surface Arctic Water is found. From the East, from the regions between Franz Josef Land and Kvitöya and between Edgeöya and Kong Karls Land (Olga Strait) water of East Spitsbergen Current (ESC) flows southwards and to the SW. In the region of Hopen Island this water divides. Part flows to the west, to enter Storfjorden and next after rounding the southern promontory of Spitsbergen (Sörkapp Current) turns to the north. Water of this current flows along western coast of Spitsbergen on the West Spitsbergen shelf, between coast of the island and water of the warm WSC (see Fig. 3.3). The second part of the cold water from the Barents Sea (where branches of the ESC and Persey Current connect in the vicinity of Hopen Island) flows southwards and SW to form the cold Björnöya Current. Both currents (Sörkapp and Björnöya) function in the shallow water zone (to the bottom of the not so deep shelf; ~100–150 m).Heat resources in Sörkapp Current waters are not big; water at a depth below 50 m during most of the year has a temperature close to zero or below zero. Salinity is variable (32–34 PSU). Similarly variable are discharges of Sörkapp Current that depend on regional atmospheric circulation.

Variability of the temperature of water surrounding Spitsbergen is further characterised by the values of monthly means of SST in two bodies of water with dimensions 2°φ x 2°λ, the centre points of which lie at the same latitude 76°N. The first encompasses the area determined by the

[5] This means that to e depths of a few hundred meters the salinity of these waters is approximately the same, the (halocline does not occur and water temperature increases very slowly and "smoothly" towards the surface without sharp changes. The lack of thermohaline stratification enables convection to reach great depths during winter, (according to Haugan (1999) to around -200 m), and thereby effect long lasting transfer of heat from the ocean to the atmosphere.

coordinates 75–77°N, 13–15°E. The average temperature of this area is assumed to be at 76°N, 14°E. This body of water is close to the entrance of Hornsund Fjord, its centre point being at the distance of 64 NM (119 km) from the station The second body of water is between 75–77°N, 25–27°E (centred at 76°N, 26°E) and is SE of Edgeöya[6] and ESE from Hornsund station. The distance from the station is 159 NM (~294 km).

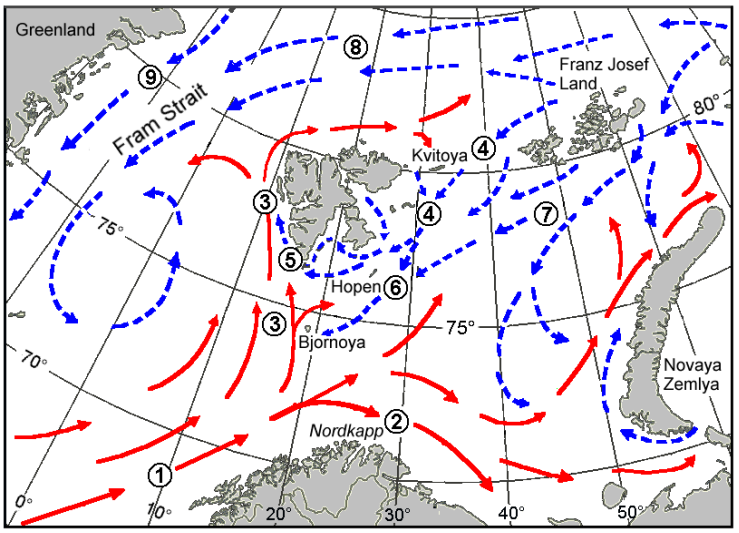

Fig. 3.3. Surface sea currents in the Svalbard region.

Currents: 1 – Norwegian, 2 – Nordkapp, 3 – West Spitsbergen, 4 – East Spitsbergen, 5 – Sörkapp , 6 – Björnöya, 7 – Persey, 8 – Trans Arctic, 9 – East Greenland.

The first body of water is characterized by its changeability of temperature at juncture of the Greenland Sea and the Norwegian Sea through which the warm WSC flows[7]. The second cold body of water is Arctic water of NW Barents Sea, part of which comes to form the Sörkapp Current and over which air masses arriving from the East can transform.

Average annual SST values are a synthesis of the resources of heat in the water. The behaviour of SST over the course of many years (1950–2009) in these bodies of water (see Fig. 3.4) will be presented next to reference them to the period of observations at Hornsund.

On the Greenland Sea at grid point 76°N, 14°E the annual water surface temperature shows over the whole 60 years long period, 1950–2009, statistically significant warming trend amounting 0.003 (±0.001)°C per year. In the initial part of the period, 1950–1972, there was a lack of

[6] Within this body of water there is Hopen Island.

[7] It is situated to the east from the main axis of West Spitsbergen Current. Annual SST to the west from this body of water is higher by around 0.7°C. The e thermal transect across the WSC is characterized by measurements at the three grids points: 10°E, 12°E and 14°E situated on the same latitude (76°N). The well-known oceanographic profile "Sörkapp" is located in this body of water Detailed research on WSC structure has been made along this transect in the last dozen years. Later (Chapter 9.3.3) data from 3 mentioned grid points will also be used.

unquestionable SST changes. After 1972 there was a sudden SST[8] drop; its minimum (2.88°C) was in 1977. From 1977–1978 to 2008–2009 there followed slow, irregular SST increases; consecutive local falls became smaller and smaller whereas increases became higher and higher. The trend of annual SST on the Greenland Sea during the last 31 years (1979–2009) is statistically highly significant; its value is 0.0233 (±0.0016)°C per year. It describes 87% of SST changeability in 1979–2009 ($F(1, 29) = 205$, $p << 0.001$).

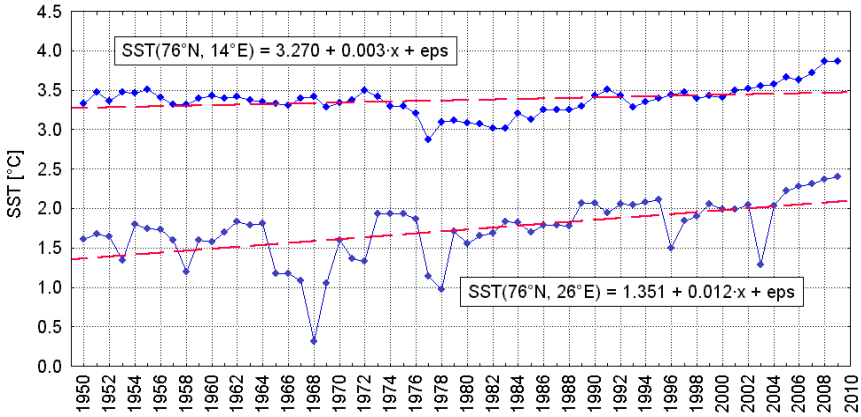

Fig. 3.4. Changes of annual SST and its trend on the western (grid 76°N, 14°E) and eastern (grid 76°N, 26°E) side of Spitsbergen.

Therefore, from the beginning of meteorological observations at Hornsund (1978) water temperature and heat resources in waters of the WSC have systematically increased. Many authors (e.g. Piechura *et al.* 2001, Saloranta and Haugan 2001, Kruszewski 2004 a, b, Styszyńska 2005, Walczowski and Piechura 2006, Walczowski 2009) have reported on the increase of water temperature in WSC, especially during the last 20 years.

On the Barents Sea (grid 76°N, 26°E) annual SST over the period 1950–2009 increased, although the scale of temperature fluctuation is significantly greater there. Very strong cooling of water in this body of water was noted at the end of decade of the 60's (particularly in 1968). At this time there was a very strong cooling in the Atlantic Arctic and growth of SIC reached dimensions similar to those at the beginning of 20th century (Divine and Dick 2006, 2007). After this cooling there were a few SST falls (see Fig. 3.4), e.g. in 1977–1978, but over the whole period the trend is positive (0.0122(±0.0024)°C/year) and statistically significant ($p < 0.0001$). The trend in this period includes around 30% of annual SST variability. In the last 31 years (1979–2009) the value of the annual SST trend on the Barents Sea is slightly smaller than SST trend on the Greenland Sea (0.0172 (±0.0042)°C/year) but also statistically significant ($p < 0.004$).

Analysis of monthly SST trends (1979–2009) in both bodies of water shows that on the Greenland Sea (76°N, 14°E) there are statistically highly significant trends in all months of the

[8] The SST temperature drop was connected with arrival of water of the first "Great Salinity Anomaly" to the North (see Häkkinen 1993, Weigand et al. 1998).

year. These are relatively strong for the winter months: 0.029(±0.002)°C in December, 0.024 (±0.003)°C in January, 0.021 (±0.002)°C in February, 0.023 (±0.002)°C in March and 0.020 (±0.002)°C in April, slightly weaker (0.018–0.020)°C in May, June and July, increasing again to 0.023–0.028°C in August, September and October. On the Barents Sea positive, significant SST trends are evident in the period from July to March. Trends from April to June are also positive but statistically not significant. The strongest trends on the Barents Sea are evident in summer months: July, August and September (0.019–0.020)°C and in October (0.021(±0.003)°C), and December (0.022(±0.005)°C). In those two last months trends on the Barents Sea attain the highest values.

Such distribution of monthly trends shows some fundamental differences in the reasons for SST increase in these bodies of water. On the Greenland Sea increase of SST first of all happens as a result of growth of heat transfer from the Atlantic water by the WSC (high and statistically significant trends in winter months), in a smaller degree as an effect of solar heat accumulation during summer warming of the ocean. On the Barents Sea the main role in the formation of SST increase is solar radiative heating, augmented as the result of SIC decrease during the warm period. This is shown by accumulation of significant positive trends with the highest values between July and the end of the year. It is symptomatic that in the Barents Sea the lowest trends (without statistical significance) occur in "spring" months or months of the turn from cold to warm season of the year (April: 0.014(±0.009)°C; May: 0.014(±0.011)°C; June: 0.014(±0.08)°C). This means that SIC melting on this body of water delays increase of SST– decreases duration of radiation access to the water surface and increases heat losses due to phase transformations of water. As a result only in the summer are there significant increases of heat reserves in this water and thus significant SST increase during summer maximum (August- September), and further quite strong SST increase during autumn-beginning of winter at average conditions of heat flux from the sea surface to the atmosphere. In such situation, the reasons for SST changes in the Barents Sea, besides advective SST increase in neighbouring bodies of water (forced by inflow of advective heat) first of all should be sought in the functioning of feedbacks between the extents of SIC, albedo changes and heat reserves in water, with participation of "ocean memory".

Average monthly water temperature in these bodies of water in 1979–2009 is shown in Table 3.6. Ranges of changeability show on Fig. 3.5 include characteristics from the 60-year period, 1950–2009. Data are from the set ER SST v.2 (Smith and Reynolds 2004).

Comparison of the plots in Fig. 3.5 shows that changes of SST in differ in the two bodies of water. The data presented in Table 3.6 show that at grid 76°N, 14°E change of SST is little but at grid 76°N, 26°E it is substantial. During the entire year the water surface of the Greenland Sea has a higher temperature than surface of the Barents Sea. Particularly big differences are found in winter. On average, in November and December water at grid 76°N, 14°E is warmer by 1.7°C than water at grid 76°N, 26°E. From January to May, water on the Greenland Sea is warmer by 1.5–1.6°C. Differences of SST between the two bodies of water decrease in the period from June to September when in both bodies of water a layer of surface water above the summer thermocline develops, strongly warmed by solar radiation. The smallest differences of SST are in August (1.05°C) and September (1.15°C).

It should also be noted during the entire year differences between SST on the Greenland Sea (grid 76°N, 14°E) and the monthly temperature of air at Hornsund (Table 3.6; row ΔtGH) are positive. This means that the water surface temperature is higher than the air temperature. The greatest

differences are evident in the cold season of the year but even in the warmest month (July) SST is little higher than air temperature at Hornsund. Differences between SST on the Barents Sea and monthly air temperature at Hornsund (Table 3.6; row ΔtBH) are clearly lower. On July SST on the Barents Sea is slightly lower (0.4°C) than air temperature at Hornsund.

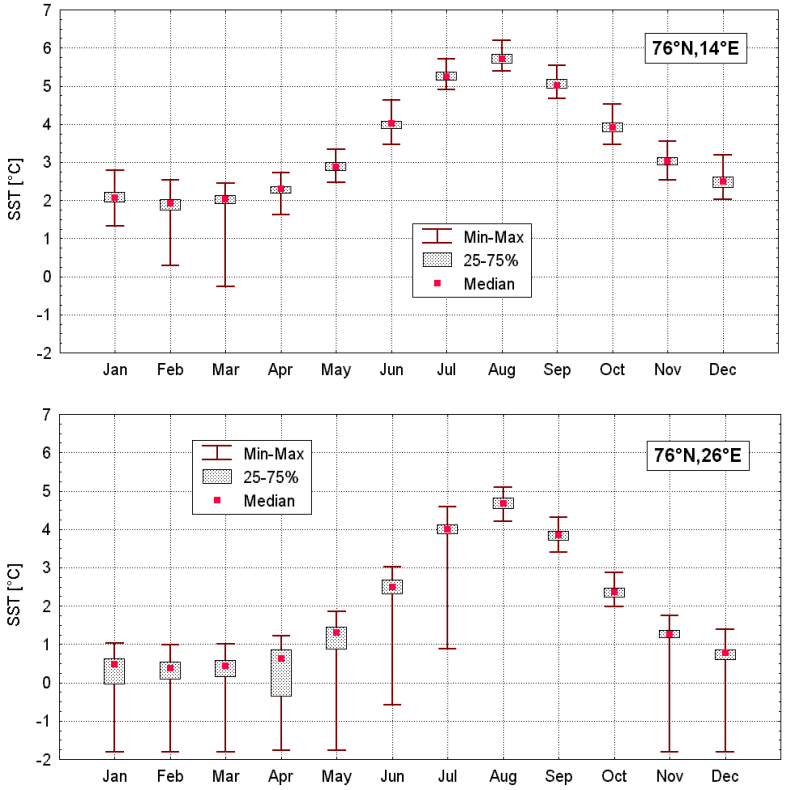

Fig. 3.5. Range of SST variability in 1950–2009 on the western (grid 76°N, 14°E) and eastern (grid 76°N, 26°E) side of Spitsbergen.

Over the longer period,1950–2009, it can be observed that the water surface at the boundary between the Greenland Sea and the Norwegian Sea there was only one month (single case – March 1977) when occurrence of a negative temperature (–0.26°C) was noted (Fig. 3.5). On the Barents Sea situations with monthly SST below 0°C were the rule from November to June.

Minimum SST higher than 1.5°C and a small range of fluctuation in the winter months proves on the great heat resources in waters of the Greenland Sea. Consecutive advections of chilly air, even together with strong winds cannot decrease SST in WSC below this limit. Heat resources are constantly refreshed there by ocean current transfers (see the next chapter). At the same time in the NW Barents Sea SST often drops below zero. This is due to the limited heat resources in this body of water. Heat resources accumulated during summer warming in the Arctic water extend only a few (at most one dozen) meters in the surface layer, to the level of the summer thermocline. After September this heat is quickly transferred to the atmosphere.

Table 3.6. The average monthly SST at 76°N, at grid points 14°E and 26°E (SST), standard deviations (σ_n) and minimum and maximum monthly temperature (SST_{min}, SST_{max}) noted on these surfaces, average monthly air temperature at Hornsund (Tm) and differences between average monthly SST and monthly temperature at Hornsund ((ΔtGH = SST on the Greenland Sea – Tm at Hornsund), ΔtBH = (SST on the Barents Sea – Tm at Hornsund), see text). Common period 1979–2009.

	Jan	Feb	March	April	May	June	July	Aug	Sept	Oct	Nov	Dec
14°E												
SST	2.07	1.90	2.01	2.26	2.86	3.98	5.27	5.77	5.08	3.93	3.01	2.35
σ_n	0.26	0.23	0.22	0.21	0.21	0.27	0.21	0.24	0.26	0.28	0.26	0.29
SST_{min}	1.58	1.51	1.65	1.95	2.47	3.46	4.90	5.40	4.67	3.46	2.53	2.03
SST_{max}	2.79	2.54	2.45	2.73	3.33	4.64	5.72	6.19	5.53	4.53	3.56	3.20
26°E												
SST	0.51	0.40	0.49	0.74	1.31	2.53	4.05	4.72	3.90	2.41	1.30	0.81
σ_n	0.33	0.41	0.38	0.47	0.55	0.43	0.23	0.23	0.22	0.23	0.21	0.30
SST_{min}	–0.62	–1.15	–0.85	–0.87	–0.77	0.61	3.60	4.21	3.41	1.99	0.91	–0.17
SST_{max}	1.03	0.99	1.01	1.23	1.86	3.03	4.58	5.09	4.32	2.87	1.75	1.38
Hornsund												
Tm	–10.9	–10.8	–10.6	–8.5	–2.8	1.9	4.4	4.1	1.4	–3.4	–6.4	–9.5
ΔtGH	13.0	12.7	12.7	10.8	5.7	2.1	0.9	1.7	3.7	7.3	9.4	11.9
ΔtBH	11.4	11.2	11.1	9.0	3.4	0.6	–0.8	0.3	2.5	5.8	7.7	9.8

Comment: Occurrence of negative SST ≤ –1.8°C within SST_{min} values means complete covering of the water body with sea ice. Maintaining of SST in the range from –1.79 to –0.4°C means that high SIC occurred on the body of water for the part of month or that the body of water during that month was covered with sea ice of concentration lower than 9+.

3.3.2. Sea ice cover

Reliable and homogenous data on the ice cover encompasses a shorter period, 1979–2007. These are satellite data, reporting on water surface ice cover equal and higher than 15% (sea ice extent SIE). Data originate from the archive of National Snow and Ice Data Centre (NSIDC)[9]. The organization of data containing monthly averages has little spatial resolution. These data are not integrated according to bodies of water in their exact oceanographic division but with regional divisions established earlier. For waters surrounding Spitsbergen in this set there are data on the monthly SIE on the Greenland Sea (together with Danish Strait) and on the Barents and Kara Seas, treated as sum of the ice surface on both these bodies of water[10]. In spite of limited spatial resolution, these data provide quite good information on the main features of seasonal and interannual variability of SIE around Spitsbergen. A common series enabling analysis of relations between ice cover and climatic parameters at the Hornsund station are 29 years in length (1979–2007).

On average, SIE on the Greenland Sea reaches its greatest extent in March, in the Barents and Kara Seas in April. Differences between average monthly SIE on each of these seas between

[9] This is a set gsfc.nasateam.month.extent.1978-2007.n, elaborated by D.J. Cavalieri from NASA; Goddard Space Flight Center.

[10] Data from the Arctic Ocean are omitted because SIC changes within this body of water, because of its great dimensions (around 8 million km^2), do not characterize changes of SIC occurring North of Spitsbergen.

February, March and April are statistically not significant. The maximum ice cover may occur in any one of these months. A clear minimum SIE is evident (in multiyear averages) in the Greenland Sea, the Barents and the Kara Seas synchronously in September. The ice cover at its maximum on the Greenland Sea (~0.9 million km^2) is nearly two times smaller than ice surface on the Kara and Barents Seas (~1.85 million km^2) but in September these differences nearly disappear and average ice surface on the Greenland Sea (0.336 million km^2) becomes nearly the same as on the Barents and Kara Seas (~0.330 million km^2).

The reason for such strong ice cover of the Greenland Sea[11] during the SIE minimum is occurrence along the eastern coast of Greenland of the belt of thick ice transported by the East Greenland Current from the Arctic Sea southwards. At the same time the Barents and Kara Seas can become ice-free almost to their northern borders. Average monthly areas of SIE in these bodies of water and values characterizing their observed variability are compared in Table 3.7. Annual sequences of SIE, 1979–2007, with the range of changes are shown on Fig. 3.6.

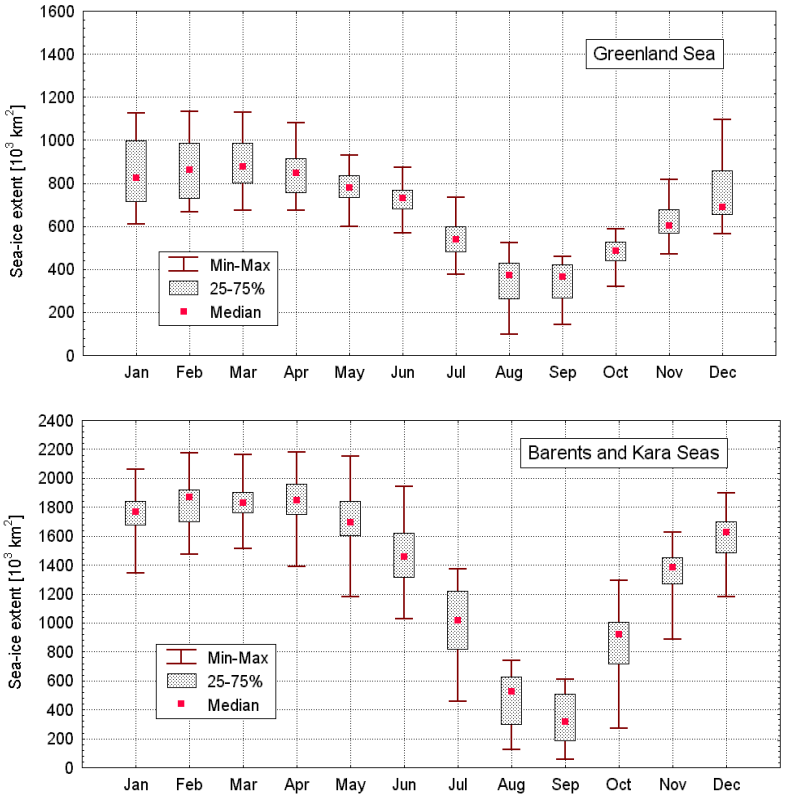

Fig. 3.6. Range of SIE variability on the Greenland Sea and the Barents and Kara Seas in 1979–2007. Scales are different on both sides of the plot.

[11] Strong in relation to the area of body of water. The Greenland Sea has an area ~1.2 million km^2, the total area of the Barents and Kara Seas is ~2.3 mln km^2.

Analysis of Table 3.7 shows that there are big differences in the character of variability of sea ice cover on these bodies of water. The biggest variations of SIE on the Greenland Sea occur in December and January, that is at the beginning of winter when ice cover first develops there. The lowest SIE variability is in May – July. The biggest SIE variation on the Barents and Kara Seas takes place in October (beginning of ice cover formation) and at the end of spring – beginning of summer (June – July). The growth of ice cover on the Barents and Kara Seas occurs much earlier, in October (Table 3.7, columns σ_n). This growth is evident mainly on the Kara Sea – the Barents Sea freezes later, in November and December. Freezing processes develop the most strongly initially in N and NE parts of these seas, spreading later in the eastern parts. The SW parts of the Barents Sea, fed with Atlantic water by the Nordkapp Current, do not freeze even during the strongest winters. In practice the differences between the area of body of water (2.3 million km^2) and SIE of the Barents and Kara Seas combined during maximum growth of ice (February, March, April) correspond to the ice-free area on this part of the Barents Sea. On the average, during the maximum SIE on the Greenland Sea ~410 thousands km^2 water remains free of ice on average and on the Barents Sea there are ~450 thousands km^2 of "clean water ". If it is taken into account that heat resources in water of the Greenland Sea during formation of ice are greater than in water in the unfrozen part of the Barents Sea, so "the warming" influence of the Greenland Sea (stronger than the Barents Sea) on the climate of Spitsbergen becomes understandable.

Table 3.7. The average monthly SIE (thousands of km^2) on the Greenland Sea and on the Barents and Kara Seas (Mean), minimum (Min) and maximum (Max) ice area on these bodies of water and standard deviations from the average (σ_n). Period of analysis 1979–2007.

Month	Greenland Sea				Barents and Kara Seas			
	Mean	Min	Max	σ_n	Mean	Min	Max	σ_n
January	842.7	611.0	1126.9	159.1	1751.0	1343.9	2060.0	165.4
February	877.5	667.8	1134.0	143.8	1819.6	1476.4	2171.9	164.4
March	891.9	673.9	1129.0	124.3	1849.9	1514.0	2161.0	138.8
April	853.5	673.5	1081.9	114.8	1850.3	1388.8	2179.1	181.9
May	785.3	598.1	929.3	83.6	1704.3	1177.8	2150.2	236.4
June	723.0	570.5	873.6	72.6	1471.3	1026.3	1944.1	216.9
July	543.6	375.4	735.7	92.6	997.9	459.8	1370.1	256.4
August	348.4	100.0	524.1	112.5	472.4	122.7	739.9	190.6
September	336.6	143.3	458.1	106.5	330.5	55.2	610.8	176.6
October	477.8	319.4	589.4	68.4	877.5	271.6	1291.3	245.2
November	618.6	470.0	816.5	85.9	1345.3	889.0	1628.9	177.0
December	753.3	566.6	1095.3	143.7	1588.8	1182.8	1896.4	180.6

In the both bodies of water, the Greenland Sea and the combined Barents and Kara Seas over the research period (1979–2007) systematic decrease of SIE is evident. Variability of SIE at the maximum growth (March) and minimum growth (September) on the Greenland Sea and Barents and Kara Seas is shown on Fig. 3.7.

On the Greenland Sea there is a statistically significant negative trend of SIE at maximum growth (March) of –9.93(±2.06) thousands km^2·yr^{-1} ($p < 0.001$). At the time of occurrence of the smallest area (September) this trend is over two times smaller (–4.15 thousands km^2·yr^{-1}) and

statistically not significant ($p < 0.079$). It may be drawn to the attention (Fig. 3.7) that on the Greenland Sea after 2000 there was a stepwise decrease of SIE in September. In the following four years, this area kept stably in its limits to around 200 thousands km^2, compared to around 400 thousands km^2 in the preceding four years[12]. After 2004 SIE started to increase again and in 2007 exceeded 400 thousands km^2.

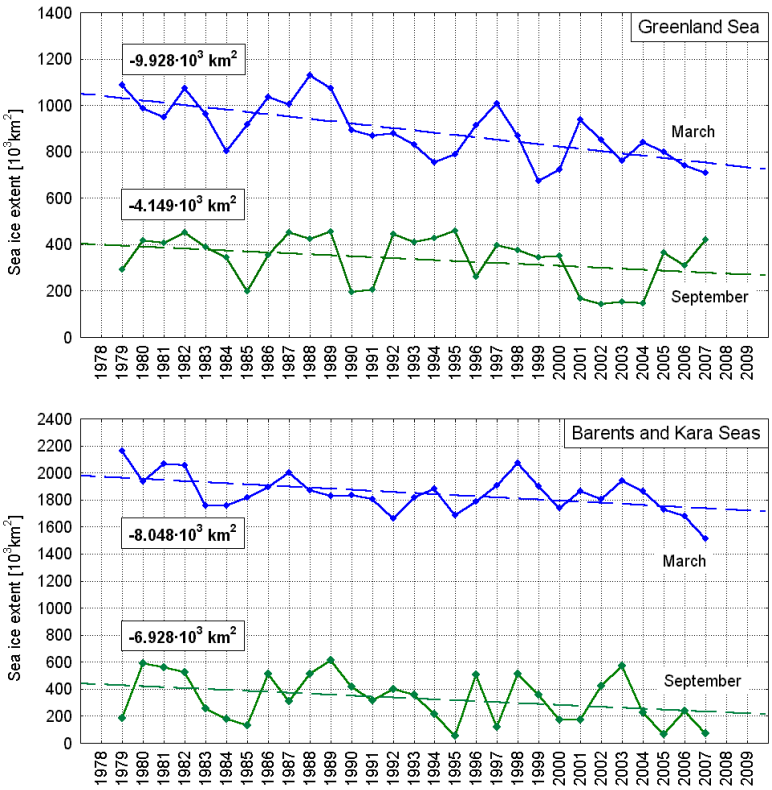

Fig. 3.7. Changes of sea ice area on the Greenland Sea and the Barents and Kara Seas during the maximum (March) and minimum (September) cover times, 1979–2007.

On the Barents and Kara Seas the strong negative trend of SIE at the minimum growth (–6.93 (±3.76) thousands km^2·yr^{-1}) is statistically not significant. This situation may be explained because during the last dozen years SIE, in result of systematic decrease of its area during September, it comes to area below 200 000 km^2 so close to the minimum below which it cannot decrease.

The declining trend of SIE changes during maximum growth (–8.05 (±2.73) thousands km^2·yr^{-1}) is stronger than the trend at the minimum. On the Barents and Kara Seas, a sudden decrease of SIE in September, similar to that which occurred after 2000 on the Greenland Sea was not

[12] This stepwise decrease of SIE on the Greenland Sea can be associated with an abrupt increase of heat resources in water of West Spitsbergen Current in 2000–2005, discovered and described by Walczowski and Piechura (2006).

evident, whereas after 2003 the accelerated systematic decrease of SIE in March is evident. Kvingedal et al. (2005) also pay attention to the different character of SIE variability on the Greenland and Barents Seas. Decrease of SIE over the entire surface of the Nordic Seas[13] between January 1967 and December 2002 is estimated to be around 15% (trend –4.1% per decade).

Observation of daily ice maps made over a dozen years allows for a general description of ice cover development in the region of Spitsbergen. At the beginning of winter or somewhat earlier (usually in November) there comes the slow growth of SIC to the east of Spitsbergen. The limit of the ice there gradually extends to S and SW, in part as a result of ice drift, in part due to local freezing. Usually in December autochthonous ice grows in Hinlopen and in Storfjorden. The edge of the ice drifting from the east-north east gradually approaches this local ice. On the Greenland Sea near to Spitsbergen coast sea ice does not occur at this time.

As SIC builds up on the eastern side of Spitsbergen and ice begins to be carried by the Bjornöya Current towards the island (this occurs usually at the turn of December and January or somewhat later in January) ice also rounds Sörkapp and is carried out into the Greenland Sea by the Sörkapp Current; the ice appears in the southern part of western coast of Spitsbergen.

If at this time the axis of the WSC moves away from the coast to the west and/or heat resources in this current are merely average and the flow of cold water of the Sörkapp Current and its ice is strong (domination of winds from NE-E, high wind velocity) there is intensive outflow and rapid drift of sea ice to the north along the coast. Fjord entrances[14] become gradually filled with drifting sea ice, beginning with Hornsund. If simultaneously air temperature is low (and usually it is)[15], this ice can freeze in fjords and can form a relatively dense cover. Drifting ice enters Isfjorden two to four weeks later after rounding Sörkapp. Next ice fills up the southern part of Forlandsundet (provided that the no stable ice was formed there earlier). To the west of Prins Karls Forland ice carried to the north still melts in January, so waters to the north of the NW tip of Spitsbergen at the beginning are free of ice. Only the drift of ice from the north and west, pushing ice from the Arctic Sea to the northern coast of Spitsbergen can gradually fills up the "embayment of clear water above 80°N that often extends to the northern limits of Hinlopen or even to Nordaustlandet. The timing of freeze of this "bay" may differ – it takes place usually in February or March. At that time along the western coast of Spitsbergen the band of drift ice widens and may attain a width in February-March of around 30–50 NM (55–90 km). The process of fast decline of the ice cover starts in April – the ice degrades, is gradually broken by waves and drifted by wind to open, warmer water and finally melts. The western coast (excluding internal parts of fjords) is usually accessible in mid-May. In the second part of May/June, the internal areas also become free of ice. Hence, on the forefield of fjords single ice floes or aggregates of sea ice floes arriving from its interior may be

[13] The Nordic Seas – name often used by Scandinavian and British researchers – the bodies of water including the Greenland Sea, water around Iceland (together with the Irminger Sea), the Norwegian Sea and the Barents Sea.

[14] Hornsund up to Treskelen, Bellsund up to Askelöya and entrance to Van Keulenfjorden.

[15] Low temperatures are connected with increase of frequency and intensity of advection from E–NE, which simultaneously are conducive for intensification of the Sörkapp Current and carrying of ice out to the western coast of Sörkapp.

encountered at that time. In July on the forefield of the western coast of Spitsbergen, sea ice is usually not observed whereas glacier ice is quite often found.

However if at the time when sea ice starts moving out with the Sörkapp Current, the core waters of the West Spitsbergen Current are shifted to the east and warm Atlantic water spreads on the Spitsbergen shelf and/or heat resources in water of West Spitsbergen Current are higher than average, ice cover development along the western coast of the island is greatly delayed. Ice carried out to the West Spitsbergen shelf by the Sörkapp Current melts very quickly.

Such strongly diminished ice, moving in a narrow belt along the coast extends in general not farther than the water body between Hornsund and Bellsund. Up to the end of winter, stable ice cover is not formed along the western coast. Ships may enter Isfjorden and Kongsfjorden without greater obstacles. During such winters, internal parts of Hornsund (Brepollen, Burgerbukta, and Samarinvagen) are covered with autochthonous ice whereas the axial part of Hornsund (up to Treskelen) remains unfrozen[16]. Only drifting sea ice with differing, on the whole small, ice concentration occurs here periodically. Conditions are similar in other fjords. The entrance, deep-water areas remain free of ice or drifting allochtonous sea ice appears periodically; internal parts of fjords remain partly or wholly frozen. In some years, after the winter SIC has left the western coast of Spitsbergen there may be some renewed development in the late spring or summer (May -July).This happens when heavy Arctic ice starts to be carried out off the Arctic Sea basin between Franz Josef Land and Kvitöya –Nordaustlandet. The drifting ice carried by the East Spitsbergen Current together with the cold (temperature around -0.5 to 0°C) and de-salinated Arctic Surface Water reaches the Sörkapp Currents and is moved to the western coastal water s. ASW together with ice moves fast to the north along the coast, filling entrance areas of Hornsund, next Bellsund and finally Isfjorden. Along the western coast of Spitsbergen, to the mouth of Isfjorden a belt of ice with differing concentration builds up. It is the widest at the western coast of Sörkappland, (up to 40 NM (75 km) here), while at Kapp Linné (the southern entrance to Isfjorden), its width is only few miles. Because this ice is thick (1.5-2.5 m) and floats on strongly cooled water its melting proceeds slowly despite relatively high air temperature[17]. Usually in such situations "summer" ice cover on the SW coast of Spitsbergen lasts from 2 to 4 weeks (Styszyńska and Wiśniewska 2002, Styszyńska and Buchert 2005). The last time during the Hornsund station operations that there was such strong "summer" drifting ice was in 2004, from the last ten days of June to the last ten days of July (Fig. 3.8). There was slightly weaker ice cover in the first ten days of July 2008.

The edges of the ice pack in these waters show great changeability from day to day and from month to month. Their positions depend first of all on the sea surface temperature distribution and the characteristics of the ice drift, the dynamic factors. In the individual bodies of water the times of maximum or minimum ice extent are asynchronous as a rule. In the NW Greenland Sea maximum extent of the ice edge in a given year was in March whereas in the SW it was in April, for example. Because of this, the data on the ice area are more precise than information on location of the ice margins.

When estimating the locations of the edges of ice pack (at the maxima and minima) the history of the ice cover development during the preceding winter or of its melting during the warm period

[16] It does not exclude formation of coastal ice along the coast of fjord and/or in the bays of this part of Hornsund, e.g. in Isbjörnhamna.

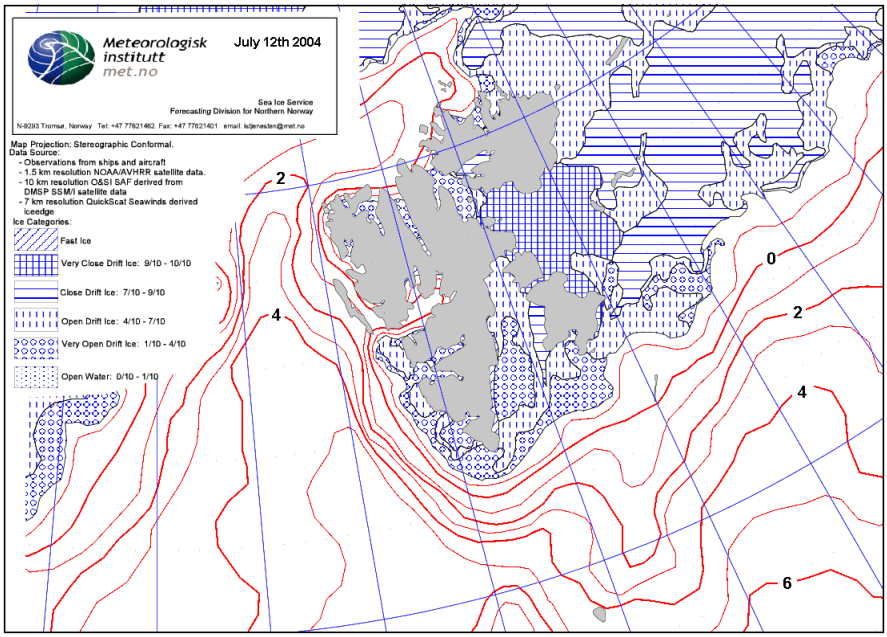

Fig. 3.8. Distribution of SST and sea ice concentration in the region of Svalbard. This map of ice cover was published by Norwegian Meteorological Institute on July 12, 2004 (http://met.no/kyst_og_hav/iskart.html).

preceding a minimum must be taken into consideration. For information on the ice extent in the best understood region of Spitsbergen, a selection of maps from the collection of Divin and Dick (2007) for characteristic times in March or April (extent close to maximum) and August (extent close to minimum) are shown. In Fig. 3.9 two such extreme situations are shown: 1) the course of ice border in March and April 1969 documents the greatest extent of ice cover in the second part of the 20th century and in the first years of the 21st century in the Atlantic sector of the Arctic; 2) the least extent in August 2001 and 2002.

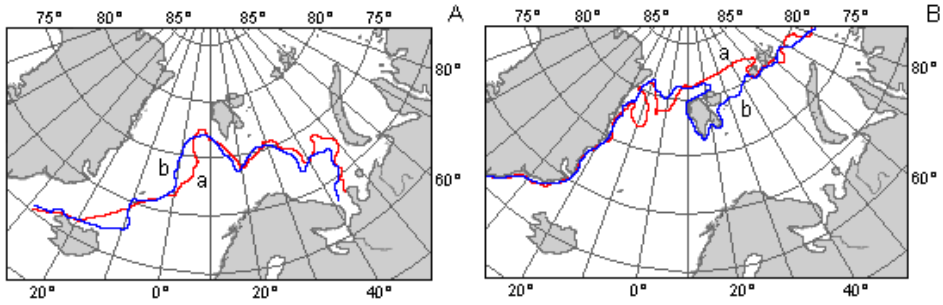

Fig. 3.9. Sea ice borders at the times of its maximum and minimum extent in the second half of the 20th Century: A – in March (a) and April (b) 1969, B – in August 2001 (a) and August 2002 (b) (after Divin and Dick 2007)

For 1979–2004 there are sound and firm data on SIC. In this period the minimum sea ice cover on the Greenland Sea (179 thousands km^2) was noted in 2002. These maps establish, regardless the temporary course of drifting ice borders, how ice growth developed from its minimum to its maximum extent in some periods, or what changes has taken place during cessation of ice cover – from maximum to minimum ice extent.

Changes of location of the ice border during the expansion and then shrinking of the ice pack in the ice season, 1983/1984, are shown on Fig. 3.10. 1984 was the second the "warmest" (after 2006) with respect to air temperature in the history of observations at Hornsund. Development of the SIC in the season preceding 1988 that was characterized by the lowest average annual air temperature (in the history of observations at Hornsund) is shown on Fig. 3.11. Comparing Figures 3.10 and 3.11 one may easily note that summer ice extent in the Atlantic Arctic gives indirect information on the degree of "severity" of approaching winter periods.

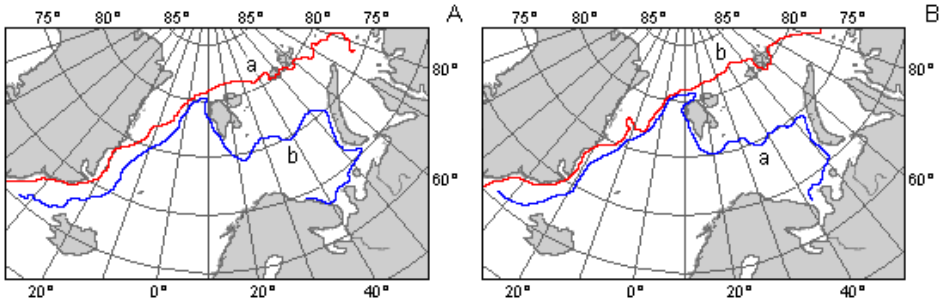

Fig. 3.10. Changes of the ice border between minimum and maximum ice cover in the Atlantic Arctic: A – August 1983 (a) and March 1984 (b), B – April (a) and August (b) 1984 (after Divin and Dick 2007).

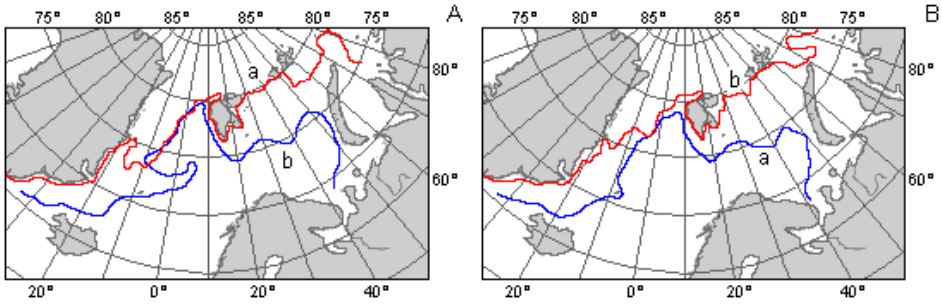

Fig. 3.11. Changes of the ice border between minimum and maximum ice cover in the Atlantic Arctic: A – August 1987 (a) and March 1988 (b), B – April (a) and August (b) 1988 (after Divin and Dick 2007).

3.3.3. Factors influencing changes of SST and ice cover in the region of Spitsbergen

The behaviour of the SIC on the Greenland Sea and the Barents and Kara Seas raises the question of the reasons which have led to the decrease of its area. Theoretical and empirical Russian research on the heat balance of sea ice melt in the Arctic (e.g. Doronin 1967, Zakharov

1981, 1987, and 1997) found that for melting the basic heat source is that in the seawater. In the existing there climatic conditions in the Arctic, the key factor conditioning the moment of beginning of freezing (besides air temperature), and thus the potential ice thickness at the end of the winter season is the existence of the picnocline (halocline). The picnocline obstructs convection in the water column. This reduces heat resources possible for transfer to the atmosphere from water above the picnocline. As a result, heat resources in the waters below the picnocline are not involved in any superficial convection, permitting the rapid drop of temperature in the water above the picnocline. In relation to thermal conditions the body of water on which picnocline occurs behaves as its depth would be equal to the depth to picnocline (Zakharov 1981, 1997). Such findings suggest that the causes of SIC changes should be sought in changes of the heat resources in water and in changes of thermohaline structure. Thus, the very important factor controlling changes of SSTas well as SIC is the heat transport in the Atlantic water flowing into the Arctic. A number of researchers note significant connections of climatic changes in the Arctic (including the present warming) with changes of heat amounts introduced into the Arctic by oceanic circulation (e.g. Polyakov *et al*. 2005, Styszyńska 2005, Dimitrenko *et al*. 2008, Semenov 2008, Jia *et al*. 2008).

These are not the only opinions on this question, however. Numerous groups of investigators ascribe the decrease of SIE in the Arctic (including the bodies of water being considered here) in equally simple and convincing terms - the SIE decrease has to be the result of the observed increase of air temperature in the Arctic and this, in turn, has to be result of the green house effect and eventually action of other factors, for example occurrence of specific types of atmospheric circulation (e.g. Stroeve *et al.* 2007, Johannessen *et al.* 2004, Johannessen 2008, Overland *et al.* 2008). Such views predominate at present. It is not so simple, however, and from the physical point of view – also not obvious. Occurrence of negative correlations between SIE and air temperature or CO_2 concentration informs us only on the existing relations between them. It does not authorize us to conclude what is the cause and what is the result.

It is not known if accelerated melting of ice is result of air temperature increase or on the contrary if the observed increase of air temperature is the result of accelerated melting and thinning of ice and decrease of its concentration (Rigor *et al.* 2002) allowing greater flux of heat from the ocean to the atmosphere. In this last case, the observed decrease of SIE and increase of air temperature may have a common cause that is other than the hypothetical direct action of the green house effect.

Rigor *et al*. (2002) show that air temperature during spring and summer in the Arctic demonstrates a relationship with the AO (Arctic Oscillation) index during the preceding winter (JFM). The explanation for this relationship Rigor *et al.* (2002) see in "seasonal memory of the prior winter Arctic Oscillation". The state of winter AO by steering ice movement leads to changes in ice concentration and determines range of ice export (discharge) to the south via the Fram Strait. The positive trend of AO evident in 1979–1998 led to decrease of ice cover concentration and decrease of its thickness, which allowed for increase of heat flux from the ocean to the atmosphere. Decrease of ice thickness and concentration during the winter leads to further increase of air temperature in the spring and summer (Rigor *et al.* 2002). In this depiction, the variability of the Arctic Oscillation would be the common cause of SIE decrease and temperature increase, while temperature increase is a consequence of decrease of ice cover area and concentration.

Unfortunately analyses of longer sequences (AO and ice 1979–2007, AO and air temperature 1950–2009) does not allow full acceptance of the arguments of Rigor, Wallace and Colony (2002), at least with reference to the Svalbard region. There are no statistically significant synchronous correlations between the SIE on the Greenland Sea or on the Barents and Kara Seas, and AO index. The same result was found for a time lag (taking the AO one year earlier than a given SIE: Table 3.8). The signs of the correlation coefficients change, reflecting the lack of any stable associations, and nearly half of the correlation coefficients are lower than |0.1|.

Table 3.8. Correlation coefficients between monthly SIE on the Greenland Sea (GS) and on the Barents and Kara Seas (BKS) and monthly AO indices in the same year (synchronous; series from 1979-2007) and asynchronous with 1 year shift (series of AO indices (1978–2006) stay ahead of SIE series (1979–2007)., Having 29 pairs of data the threshold of statistical significance for this time series ($p < 0.05$) is a correlation coefficient ≥ |0.38|.

Sea Ice Extent	Jan	Feb	March	April	May	June	July	Aug	Sept	Oct	Nov	Dec
GS synchronic	–0.11	0.01	0.12	0.05	–0.10	–0.32	0.19	0.32	0.01	0.14	–0.07	–0.21
BKS synchronic	–0.35	0.04	–0.06	0.05	–0.28	–0.05	0.23	–0.07	–0.08	–0.26	0.05	–0.05
GS asynchronic	–0.27	–0.21	–0.14	–0.06	–0.21	0.23	0.06	–0.06	–0.01	–0.35	0.02	0.01
BKS asynchronic	–0.13	–0.11	0.05	–0.24	–0.17	–0.18	–0.27	–0.05	–0.05	–0.10	0.09	–0.10

Similarly weak are the statistical associations between winter AO index and air temperature. At the Svalbard meteorological stations with long observational series of air temperature (Jan Mayen, Björnöya, Hopen, Svalbard-Lufthavn, Ny Ålesund) significant correlations between average winter AO index and air temperature from April to September are not observed at all, or appear in different months (most frequently in April and/or June) as very weak positive associations ($r = 0.26–0.32$). Analysis of the scatter plot of such associations suggests that its significance is decided by outlying values, which work as levers. Thus one cannot consider that the thesis that the winter AO directs the variability of SIE and summer air temperature in the region of Spitsbergen is proven.

Other researchers see the causes of ice regime changeability in the Atlantic sector of the Arctic as results of changes of atmospheric circulation, although not necessarily connected with the Arctic Oscillation (AO) or North Atlantic Oscillation (NAO). Rogers *et al*. (2005) noted the correlation between increase of frequency of barometric lows over the Fram Strait and moderate ice conditions on the Greenland Sea and air temperature over Spitsbergen. Greater ice coverage of the Greenland Sea and stronger outflow of ice from the Arctic occurs in situations when frequency of cyclones over the Barents Sea increases. The results of Rogers *et al*. (2005) investigations are not in conflict with other results of the most recent research.

Wu *at al.* (2006) ascribe variability of the ice regime in the Arctic to a so-called "Arctic dipole ", which is the reverse of the state of atmospheric pressure over the frontier of the Kara and Laptiev Seas and over the Canadian Arctic and Greenland. Occurrence of lower pressure over the frontiers of the Kara and Laptiev Sea, with corresponding pressure increase over the Canadian Arctic and Greenland (positive phase of dipole) increases the southerly export of ice through the Fram Strait and intensifies the inflow of ice and advection of cooled air from the Arctic Ocean to the Barents Sea, simultaneously reducing of the whirlpool-like circulation of the Beaufort Sea. The opposite situation (higher pressure over the Laptiev and Kara Seas, lower over Canadian Archipelago;

negative phase of dipole) strengthens ice movement in the Beaufort Sea, which causes increase of ice concentration and thickness in the Arctic Ocean basin and reduces ice export to the south. As a result the ice area on the Greenland and Barents Seas is reduced. Wu *et al*. (2006) show that regulation of ice area by the Arctic dipole has nothing in common either with the Arctic Oscillation or with the Barents Sea Oscillation described by Skeie (2000). The mere formation of the "Arctic dipole" is result of common interaction of the ocean, atmosphere and sea ice in the Barents Sea sector.

Variability of SIE in the seas surrounding Spitsbergen shows stronger associations with the NAO than with the AO. These are without exception asynchronous associations. Immediately after a winter (December-March), during which the Hurrell's NAO index attains positive values, SIE on the Greenland Sea increases in August ($r = 0.55$), September ($r = 0.49$) and October ($r = 0.49$). Analysis of the mutual correlations of the NAO indices characterising atmospheric circulation in the Atlantic circulation sector (preceding variable), and SIE on the Greenland Sea (delayed variable) shows that between the NAO indices (annual index NAO CRU and Hurrell's NAO index) and SIE from January to March positive correlations occur with one year or two years of delay (Marsz 2007). In March of the next year, after a year with a positive NAO CRU index, SIE on the Greenland Sea increases ($r = 0.44$). In March two years after a winter (December-March) with positive Hurrell's NAO index, SIE also increases in area ($r = 0.40$). Such behaviour indicates some inertial links in the relationship between SIE on the Greenland Sea and atmospheric circulation. On the Barents Sea, immediately after a winter with positive Hurrell's NAO index (December-March) SIE at its maximum (April) is slightly reduced ($r = –0.40$, $p < 0.035$). This is to a large degree an effect of wind activity restricting ice drift to the south and south-west rather than a result of augmented air temperature (Marsz 2007)

Sorteberg and Kvingedal (2006) discovered similar, weak and overall insignificant correlations between the NAO index and winter SIE on the Barents Sea. They found considerably stronger associations of SIE on the Barents Sea with prevailing wind directions and cyclone frequency over East Siberia (!) and western parts of the Nordic Seas. At the same time the ice extent shows 1-2 years delay in relation to variable cyclone activity. The main mechanism, which according to Sorteberg and Kvingedal (2006) may explain the delayed impact of varying wind activity and cyclone frequency on SIE in the winter, is its control of the amounts of warmer water transported to the Nordic Seas and duration of transport of water with variable heat resources from the Nordic Seas to the Barents Sea.

These conclusions of Sorteberg and Kvingedal (2006) are confirmed in the earlier results of Styszyńska (2005), who showed correlations between air temperature in the Atlantic Arctic and SIE on the Greenland Sea and the Barents and Kara Seas and heat transport together with the Atlantic water carried by Norwegian Current and next West Spitsbergen Current. Styszyńska (2005) investigated associations between the index characterizing heat resources in water carried by the North Atlantic Current to the Norwegian Current in the Faeroe-Shetland Channel[17], and SIE

[17] Coordinates of the centre of this surface are 62°N, 4°W. Monthly SST data originated from NOAA NCDC ER SST v.1 set (Smith and Reynolds 2003). The Atlantic water, which comprises the Norwegian Current, next the West Spitsbergen Current and Nordkapp Current, is introduced into the Arctic in its fundamental mass when it crosses the upper part of deep water Faeroe-Shetland Channel. The set ERSST v.1.ends in June 2005, on its place NOAA NCDC introduced set ERSST v.2. (Smith and Reynolds 2004). Between

on the Greenland Sea and the Barents and Kara Seas and the air temperatures of Spitsbergen. These associations proved to be highly statistically significant and the analysis showed on the dominant role of processes of natural variability in the development of climate changes in the Atlantic Arctic in 1982-2002.

The SST of the West Spitsbergen Current and also SIE of the Greenland Sea and the Barents and Kara Seas are strongly connected with SST changes in the Norwegian Current. Increase of SST in the latter is accompanied by decrease SIE and increase of SST in the western coasts of Spitsbergen and in the central portions of the Barents Sea, and also somewhat weaker and delayed increase of SST on the north-western parts of the Barents Sea. The region where the Norwegian Current splits into two branches – the West Spitsbergen Current directing Atlantic waters to the eastern parts of the Greenland Sea and the Nordkapp Current directing them to the Barents Sea is located NW of Lofoten. Approximate coordinates before bifurcation of the Norwegian Current are 67– 69°N, 7 – 9°E (Fig. 3.3), that is around 8 – 10° to the south of Spitsbergen (~1000 – 1200 km). The average SST in the region before bifurcation in January-April (i.e. winter cooling of water centered around grid 68°N, 8°W (later LF_{1-4}; Fig. 3.12) may be an indirect signal

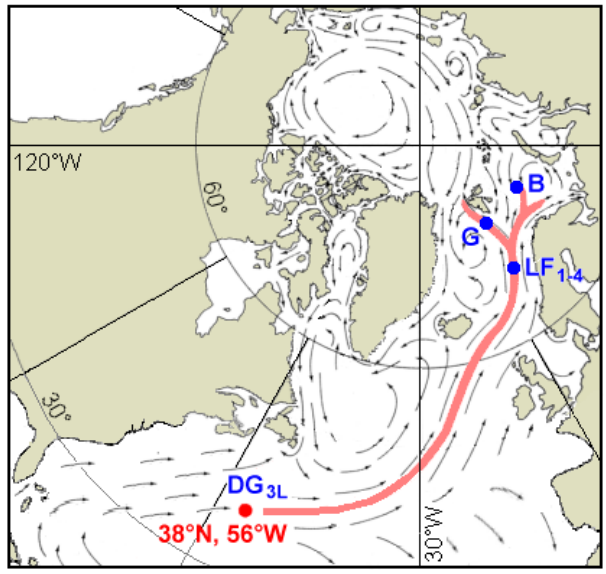

Fig. 3.12. Location of grid 38°N, 56°W, from the SSTof which the DG_{3L} index is calculated from the background of the North Atlantic Current and the Norwegian Current. Marked is location of grid 68°N, 8°E, from the SST of which LF_{1-4} index is calculated and the region 76°N, 14°E (G – the Greenland Sea, West Spitsbergen Current) and 76°N, 40°E (B – central part of the Barents Sea).

data in the set ERSST v.1. and ERSST v.2. there are such big SST differences in the Faeroe-Shetland Channel that data from the set ERSST v.2. do not confirm the existence the strong associations discovered by Styszyńska (2005). In this work SST data from the set ERSST v.2., containing data up to December 2009 are used. At present (after 2009) the set ERSST v.2. is not continued, SST data are contained in the set NOAA NCDC ERSST v.3b. (Smith *et al.* 2008, Xue *et al.* 2003).

of the changes of heat resources being transported by the Norwegian Current further into the Arctic. Higher than average SST during the winter cooling period testify to augmented heat resources in the subsurface, isothermal water layer. SST conditions during the summer do not give any information on the heat resources in the deep water, only registering water temperature above the summer thermocline. These heat resources are the result of the accumulation of solar radiation during the varying weather conditions, which succeed the winter cooling of the ocean surface.

Correlations between $LF_{1\text{-}4}$ and the annual SST of the West Spitsbergen Current in the Hornsund region (76°N, 14°E) are strong but only reach a maximum value (r = 0.88) after a one-year delay . This delay may be interpreted as a result of the passage of time necessary for the transport of heat together with the water from ~ 68°N, 8°E to ~ 76°N, 14°E. Associations between the $LF_{1\text{-}4}$ index with monthly values of SST at 76°N, 14°E in the following year are shown in Fig. 3.13. In all months of the succeeding year, these associations are very strong and highly significant ($p << 0.001$), reaching between September and December ($r > 0.86$), with the maximum in October (r = 0.90). This means that in the first year after a year in which $LF_{1\text{-}4}$ index attains higher than average values, SST in the West Spitsbergen Current will be also distinctly higher, particularly in autumn and the beginning of winter. This will cause lessening and delay in formation of sea ice along the western coast of Spitsbergen and increase of heat flux from the sea surface to the atmosphere. Thus, air temperature will increase in the Spitsbergen region, including Hornsund. Such a sequence of events is confirmed by statistical analyses.

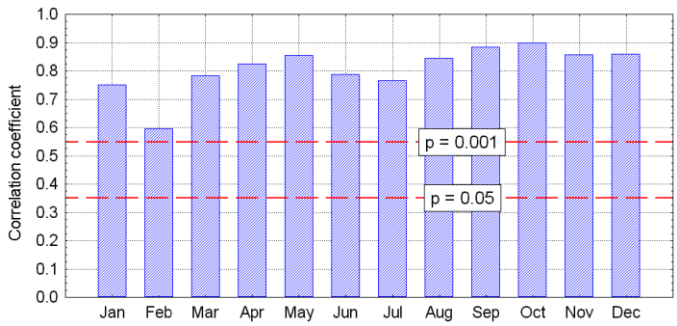

Fig. 3.13. Distribution of correlation coefficients between the heat resources carried by the Norwegian Current to the Arctic ($LF_{1\text{-}4}$; 1978–2008) and monthly SST at grid 76°N, 14°E in the next year (1979–2009). Marked are levels of statistical significance p = 0.05 and p = 0.001.

Correlations of $LF_{1\text{-}4}$ with monthly SIE on the Greenland Sea, when delayed (lagged) in relation to $LF_{1\text{-}4}$ for one year are negative in all months, statistically significant at $p < 0.05$ (Fig. 3.14). The strongest correlations are in the first months of the year – from January to May. This means that with the beginning of the year following a year in which $LF_{1\text{-}4}$ values are higher, SIE on the Greenland Sea decreases, including during the month of March (the period of maximum SIE development (Fig. 3.15), enabling earlier accumulation of solar heat by the ocean surface. The second, weaker maximum of correlation is evident in November and December. This shows up as a delay in ice formation in the preliminary phase of winter, being the result of increase of

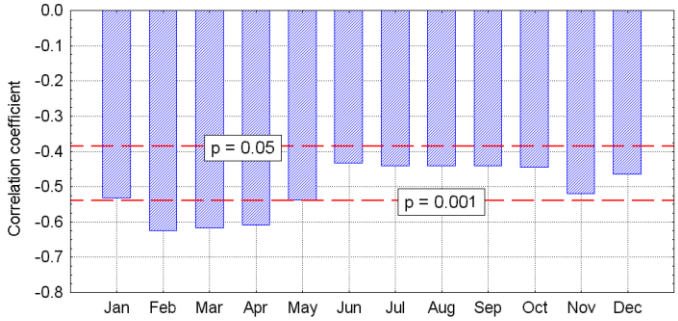

Fig. 3.14. Distribution of correlation coefficients between LF1-4 (1978-2006), and monthly SIE on the Greenland Sea time-lagged for one year (1979-2007). Levels of statistical significance $p < 0.05$ and $p < 0.005$ are marked.

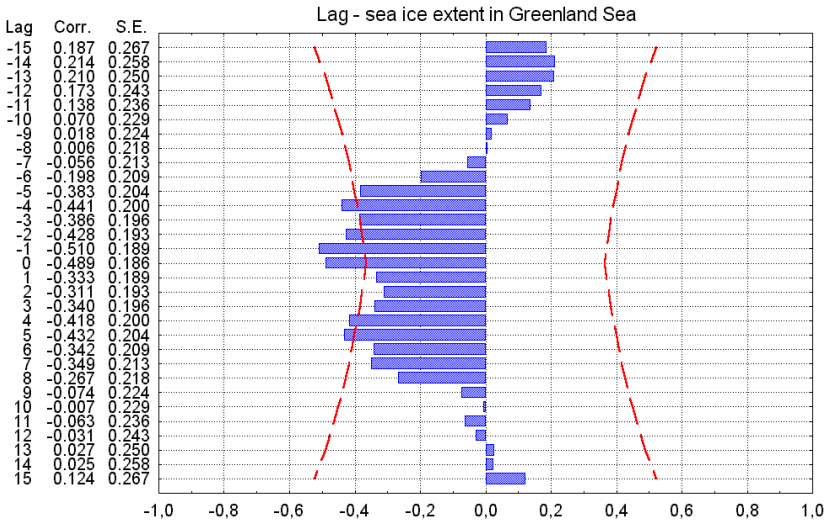

Fig. 3.15. Mutual correlations between LF_{1-4} (preceding variable; 1979-2007) and SIE on the Greenland Sea during the maximum extent of sea ice development (March; delayed variable: 1979-2007). Limits of statistical significance are marked $r < 2$ S.E. One year lag of the strongest SIE reaction and extended in time negative influence of increased heat resources in water of the Norwegian Current on maximum SIE on the Greenland Sea are seen. A seven years periodicity occurs also [–1,+5] but will be not discussed in the present work.

advective heat resources in the Norwegian Current and heat accumulated by the water free of sea ice cover in the summer.

Steering of SST and SIE changes in the Greenland Sea by changes of heat resources carried by the Norwegian Current (LF_{1-4}) to the West Spitsbergen Current is reflected in the variability of air temperature at Hornsund. The mean annual temperature at Hornsund is strongly and significantly ($r = +0.69$, $p < 0.001$) correlated with the year earlier value at LF_{1-4} (Fig. 3.16). The association between these values is linear (Chapter 9, Fig. 9.21). Correlations between LF_{1-4} and the lagged for one year monthly air temperatures at Hornsund are without exception positive and statistically

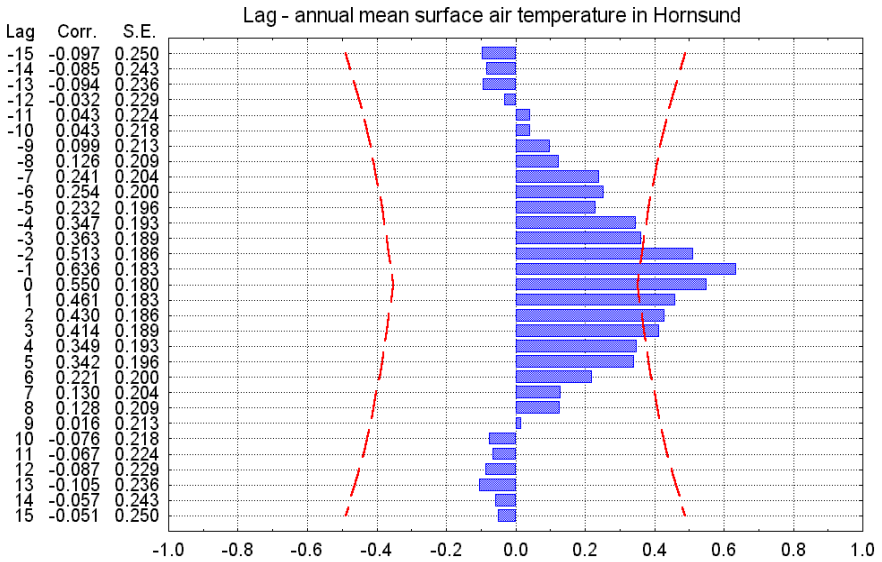

Fig. 3.16. Mutual correlations between $LF_{1\text{-}4}$ (proceding variable; 1979-2009) and mean annual air temperature at Hornsund (delayed variable, 1979-2009). Limits of statistical significance r < 2 S.E. are marked. Yearly delay of temperature reaction at Hornsund in relation to $LF_{1\text{-}4}$ is clearly seen.

significant for most of the months (Fig. 3.17) The strongest correlations are in December (r = 0.52, p < 0.003), slightly weaker (r ~+0.4 to +0.5) in January, February, May, June, August, September and November.

Similarly strong but more extended is influence of variable heat resources carried by the Norwegian Current ($LF_{1\text{-}4}$) on the SST and SIE of the Barents and Kara Seas. Correlation coefficients of annual SST in the central part of the Barents Sea (area 2 x 2°, with central coordinates at 76°N, 40°E) are statistically significantly correlated with signal $LF_{1\text{-}4}$ for the following three years. The coefficients are not so high – same year SST in the central part of the Barents Sea correlates with $LF_{1\text{-}4}$ at the +0.50 level, in the next year (one year delay also at the +0.50 level, (p < 0.004), with two years delay at 0.38, i.e. slightly higher than the limit of statistical significance at p = 0.05. In mean monthly values in the first two following year, $LF_{1\text{-}4}$ correlations of SST with $LF_{1\text{-}4}$ achieve their maximum values in September (r from 0.68 to 0.71) and October (r ~0.65). Correlations of $LF_{1\text{-}4}$ with SIE on the Barents and Kara Seas also show greater timelags than on the Greenland Sea. The characteristic feature of the $LF_{1\text{-}4}$ correlation with SIE is lack of significance of associations in August, September, October and November in the given $LF_{1\text{-}4}$ year (r from –0.15 to –0.37, n = 28) and in August, September and October one year later. The closest correlation between $LF_{1\text{-}4}$ and SIE on the Barents and Kara Seas occurs with the one year delay, in December (r = –0.68, p < 0.001). From this perspective, the correlation of conditions at $LF_{1\text{-}4}$ with SST and SIE on the Barents and Kara Seas suggests that in these bodies of water increased inflow of heat in the Atlantic water contributes to the increase of SST. Increase of SST in turn causes reduction of SIE, reduction of SIE leads to increased heat accumulation in the water and thus to increase of SST at the end of summer/beginning of autumn, which delays the development of new ice cover.

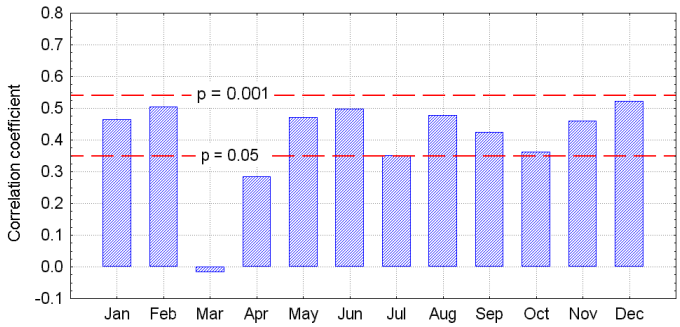

Fig. 3.17. Distribution of correlation coefficients between heat resources carried by the Norwegian Current to the Arctic (LF_{1-4}; 1978–2008) and monthly air temperature at Hornsund in the following year (1979–2009). Levels of statistical significance p = 0.05 and p = 0.005 are marked.

The nature of these interrelationships between the signals characterizing inflow of heat with the Atlantic water to this part of the Arctic (LF_{1-4}) and SIE as well as SST changes on the seas surrounding Spitsbergen (including occurrence of characteristic timelags between LF_{1-4} and both SST and SIE) shows that the factor forcing variability of SST and SIE, and also air temperature in the area[18], is inflow of heat and salts carried to the Atlantic Arctic by the oceanic circulation. The varying amounts of heat (increased – decreased) in the Atlantic water transported by the Norwegian Current causes concordant changes of SST on the Greenland and Barents Seas of around one year, and a greater delay in the Kara Sea. Changes of the amount of heat (increase – decrease) in these seas causes changes of SIE with the opposite sign. The total changes of SST and SIE force the changes of air temperature. Thus it is not changes of air temperature that cause SIE changes in the Greenland, Barents and Kara Seas but the contrary – changes of SST and SIE are reason of air temperature changes. Because changes of air temperature and SIE on the Greenland, Barents and Kara Seas have a common control, changes of air temperature at the Spitsbergen stations and changes of SIE display statistically significant synchronous correlations for most of the months.

A more accurate description of the sequence of events caused by increase of the amount of heat carried into Arctic waters by the Norwegian Current (LF_{1-4} increase) is as follows. Surface expansion of the Atlantic water limits the areas in which a layer of lower density (picnocline) sea water can occur. This enlarges the surface from which the heat resources of the deeper waters may participate in the exchange of heat between the ocean and the atmosphere. Increase of the amount of heat transported by the Norwegian Current, as indicated by SST increase in the period of winter cooling in a given year k causes (with a delay of few months at the beginning of year k+1) a SST increase in the eastern part of the Greenland Sea and in the Barents Sea. The advective heat contained in the water reduces development of the SIE during its time of maximum growth

[18] Correlation coefficient of $LF_{1-4\ series}$ from 1978–2008 with annual air temperature from 1979–2009 (one year delay) at stations Svalbard-Lufthavn, Björnöya and Hopen is equal 0.70 ($p < 0.0001$; $r^2 = 0.49$), at Ny Ålesund station is equal 0.66 ($p < 0.0001$, $r^2 = 0.44$). Earlier changes LF_{1-4} explain in this period 49–44% of annual changeability of air temperature in the Spitsbergen region.

(March, April) and next accelerates the melting of the ice. During the spring and beginning of summer in year k+1 the concentration of ice decreases and greater areas of water become free of ice earlier. As a consequence, in the spring of year k+1 the average amount of insolation reaching the open sea surface increases and the ice cover diminishes faster. A result of earlier release of the sea surface from its ice cover is the decrease of radiation losses due to reflection (ice albedo) and the phase transformations of the water.

Insolation is greatest between May 15 and July 26[19], so that each day of reduced ice cover during this period (and particularly before the moment of maximum solar declination) contributes to a significant increase of heat accumulation in the water, increasing its temperature above the "mean" and forming the summer thermocline laying on the small depth. Thus in the spring during the faster dissapearance of the ice cover air temperature over the sea increases. Increased accumulation of solar heat in the water decreases the depth of summer thermocline. Water laying below summer thermocline containing advective heat looses contact with the atmosphere, and its heat is not lost by exchange with it but instead is transported further to the north with the current. This heat next contributes to an increase of temperature in the Arctic Intermediate Water (Polyakov *et al*. 2004)[20]. Therefore, in the summer, in the face of small differences between SST and air temperature, the increase of air temperature over the ice-free sea is weak. After such a summer in the eastern part of the Greenland Sea and in the Barents Sea, SST is higher than earlier and the SIE minimum is smaller. As may be supposed in the summer of year k+1 warm Atlantic water reaches the northern parts of the Kara Sea and diminishes the ice cover still remaining there.

Increased heat resources in the water delay the growth of ice cover in autumn, especially in November of year k+1 when SIE is smaller than average. In autumn as the air temperature declines the heat flux from the sea surface to the atmosphere is intensified. This reduces falls of air temperature and thus is the next factor limiting growth of ice. Air temperature in the autumn of year k+1 becomes higher than the mean. At the moment in the autumn when heat accumulated in the water above the summer thermocline becomes exhausted, any further flux of heat from the ocean is at the expense of advective heat reserves. Reduction of SIE from September of year k+1 to its end is also the reason for SIE decrease in thickness and concentration in the initial phase of winter in year k+1/k+2 (December, January). In such situation (very big temperature differences between the sea surface and the atmosphere) heat flux from the sea may reach very large values, causing strong increases of air temperature. This limits ice growth later in the winter of year k+1/ k+2, contributing to further decrease of its thickness and f density, making it easy to predict the effects in the spring of year k+2.

Concurrent with processes occurring in year k+2 being the continuation of SST and SIE changes in year k+1, in year k+2 water passing through region LF in year k+1 reaches the Greenland and Barents Seas If in the following year temperatures in LF_{1-4} are equal to or higher than those in the preceding year the whole cycle recurs. If in year k+1, $LF1_{-4}$ temperatures are lower than in year k, warming in the Greenland and Barents Seas in year k+2 will continue, and the processes inhibit

[19] That is when Sun declination at Latitude 77°N is greater than 19° (the "flat" segment of sinusoid culmination).

[20] Increase of temperature of the Arctic Intermediate Water and restriction of bodies of water areas on which the halocline appears is a reason for decrease of sea ice cover in other sectors of the Arctic that follows with the lag (Marsz 2007).

the decrease of SIE and stabilization of SST and air over it will begin only in year k+3. A simple regression model shows that to reverse the direction of changes from the warming of the Spitsbergen region to "cooling" LF_{1-4} values should decrease distinctly for at least the three following years; only then will SIE begin to increase, SST and air temperatures to decrease. In brief the processes described here are characterized by a great inertia.

Knowing value of LF_{1-4} for year k, which may already be obtained in May of that year, we may quite reliably estimate SIE in the Greenland Sea in March of year k+1 and, more roughly, in September. Also mean annual air temperature at Hornsund (and at other Svalbard stations) may be estimated reliably for year k+1 and the air temperature that will occur in some months of both years k and k+1. Thus for the principal explanation of both decrease of SIE in the Greenland Sea, its increase of water temperature and the increase of air temperature, (effects that are especially strong in autumn and in the beginning of winter but considerably weaker in spring), we may consider increase of heat advection from lower latitudes occurring with the transport of Atlantic water by the ocean currents. Increase of air temperature in summer is the result of reducing "losses" of net insolation due to reduced need to melt sea ice; it is only indirectly controlled by variability of heat inflow with advection of Atlantic water at that season.

Progressive increase of SST of the Greenland, Barents and Kara Seas, being the cause negative trends of SIE in these bodies of water and increase of air temperature over them, is determined by oceanic processes occurring far from the Arctic. Oceanic activity in the subtropical regions of the Northern Atlantic (in the region of the Gulf Stream delta) determine the heat resources supplied by the Atlantic water to the Norwegian Current and so transported to the Arctic. Research has shown that SIE and air temperature in the entire Arctic are most strongly correlated with SST changes in the area 36–40°N, 44–58°W, centred at 37–39°N, 55–57°W (coordinates of centre 38°N, 56°W; see Fig. 3.12) (Marsz and Styszyńska 2005, 2009). Patterns of SST behaviour within the area 36–40°N, 44–58°W are very strongly intercorrelated. There are also strong correlations between SST trends in this body of water and the 1 PC (principal component) of annual SST in the Sargasso Sea (R= +0.78; n = 130). This body of water is located directly south and west of the Gulf Stream delta where the quantities of tropical water to be directed to the North Atlantic Current are regulated (Baryshevskaya 1979, Baryshevskaya and Shubenko 1983).

For standard estimation of the amount of heat contributed from the tropics to the North Atlantic Current Marsz and Styszyńska (2009) applied the DG_{3L} index. Detailed justification of construction of this index may be found in their paper. It takes the weighted mean SST in February, August and September at grid 38°N, 56°W (marking DG) from three selected years – two years earlier (k-2), one year earlier (k-1) and the given year (k) and is dated for that given year (k)[21]. Construction of this index takes into account long time needed to propagate the signal from subtropical regions to high latitudes, the losses of heat from water to atmosphere along the route, and the associated suppressing of signal amplitude, uneven velocity of water transport and other factors. Like LF_{1-4}, the DG_{3L} index is not a physical quantity but a signal carrying information on changes of the

[21] This index is calculated as follows $DG_{3L}(k) = 0.25 \cdot DG(k-2) + 0.33 \cdot DG(k-1) + 0.42 \cdot DG(k)$, where: DG(k) = (SST_Feb(k) + SST_Aug(k) + SST_Sep(k))/3; k – consecutive number of the year, SST from the surface 37–39°N, 55–57°W (coordinates of centre 38°N, 56°W); source of data – set ERSST v.2. Values of DG_{3L}, expressed in °C, are standardized according to the mean from 1901–2000 to obtain a non-dimensional form.

amount of heat being transported by the oceanic circulation from the Gulf Stream delta northwards. The chronological series of DG_{3L} indices for 1955-2009 are strongly correlated ($r = 0.79$, $n = 55$, $p < 0.000\ 001$) with anomalies of annual heat resources in the North Atlantic. This proves that variance of DG_{3L} renders the variability of the thermal state of the North Atlantic very well.

The DG_{3L} index shows very strong and highly significant correlations with the one year lagged LF_{1-i} index (Fig. 3.18) and explains 68% of its variation, 1978–2009. With the one year delay, the DG_{3L} index correlates strongly with annual SST of the West Spitsbergen Current ($r = 0.68$, $p < 0.0001$) and of the Barents Sea ($r = 0.66$, $p < 0.0001$). This index is also strongly connected with lagged monthly values of SIE on the Greenland Sea (Fig. 3.19) and on the Barents and Kara Seas (Fig. 3.20). The Index DG_{3L} is highly (r ~0.6– 0.7) and significantly correlated with annual air temperature at the Spitsbergen stations. In the series from the last 31 years (1978–2009) statistically significant

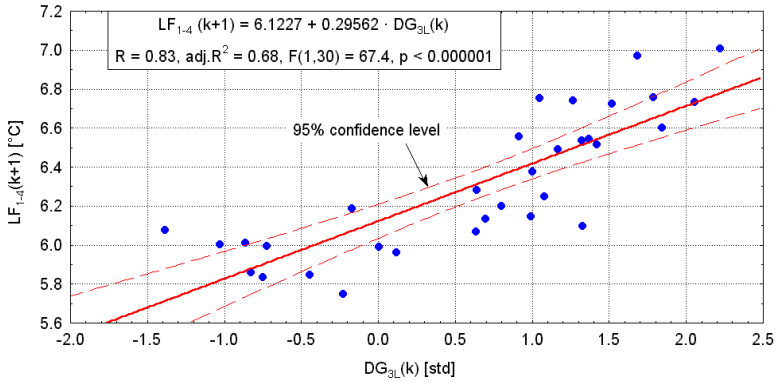

Fig. 3.18. Relationship between the index characterizing heat resources of the North Atlantic tropical water directed northwards in the Gulf Stream delta ($DG_{3L}(k)$) and the one-year lagged index for heat resources conveyed by the Norwegian Current to the Arctic ($LF_{1-4}(k+1)$).

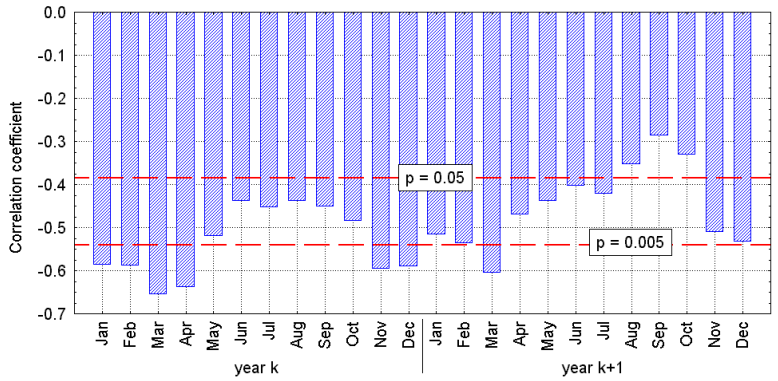

Fig. 3.19. Distribution of correlation coefficients between index DG_{3L} (year k-1) and for the one year lag (k) and two years (k+1) monthly SIE on the Greenland Sea, k – consecutive number of year. Analysis: DG_{3L} years 1978–2008, SIE – years 1979–2009. Gaps in data were removed in pairs, correlations include 26 pairs in both series. Marked are levels of statistical significance $p = 0.05$ and $p = 0.005$.

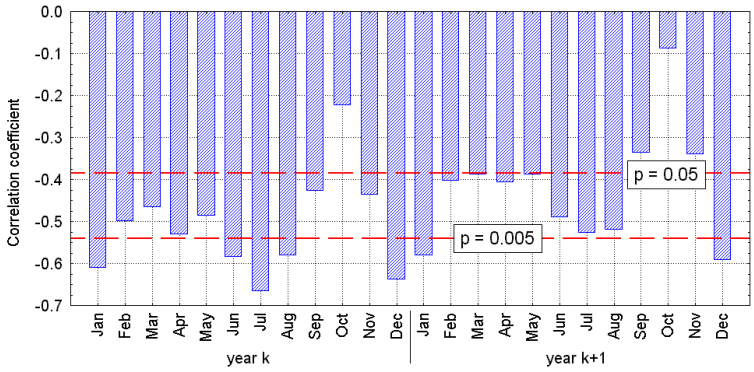

Fig. 3.20. Distribution of correlation coefficients between index DG_{3L} (year k-1) and the one year lagged (k) and two years (k+1) monthly SIE on the Barents and Kara Seas, k – consecutive number of year. Analysis: DG_{3L} years 1978–2008, SIE – years 1979–2009. Gaps in data were removed in pairs, correlations include 26 pairs in both series. Marked are levels of statistical significance p = 0.05 and p = 0.005.

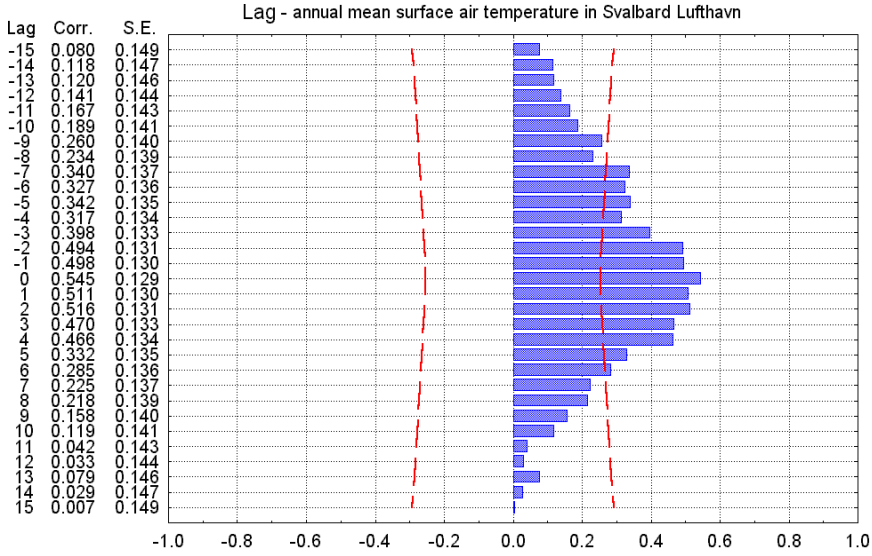

Fig. 3.21. Distribution of intercorrelations between index DG_{3L} (preceding variable) and annual air temperature at the station Svalbard-Lufthavn (delayed variable). Common period of both series is 1950–2009. Limits of statistical significance r < 2 S.E. are marked.

correlations of air temperature with DG_{3L} appear in three consecutive years. Over a longer series in which there are periods of decrease as well as of increase of air temperature (1950–2009), the correlation coefficients are slightly lower (Fig. 3.21), but significant correlations may extend for a period of few, or even of a dozen, years.

The occurrence of such strong, time-lagged relationships between the DG_{3L}, LF_{1-4} indices and SST in the Barents Sea and West Spitsbergen Current (Fig. 3.12) shows unambiguously that we have here a uniform process of meridional transport of heat with the water being a manifestation

of the Meridional Overturning Circulation (MOC). The DG_{3L} index is very strongly connected with values of the non-steady AMO annual index (Atlantic Multidecadal Oscillation); the correlation coefficient, without de-trending[22] is 0.71 ($p << 0.0001$), whereas with the series de-trended[23] it is 0.55 (1880–2009; n = 130). This allows us to interpret the changes of SST, SIE and air temperature in the region of Spitsbergen (and generally in the Atlantic Arctic), as first of all results of AMO activity. Clear recognition of the AMO signal in changes of heat resources in the Barents Sea (Kola Section) was shown by Skagseth *et al.* (2008). Similarly Chylek *et al.* (2009) found strong AMO signal control in variability of air temperature in the Arctic. Marsz and Styszyńska (2009) showed that the DG_{3L} index, being very strongly connected with the AMO index, explains for the 130 years (1880–2009) 56% of variation of air temperature anomalies in the Arctic (zone 64–90°N; data GISSTEMP, set ZonAnn.Ts.txt).

The trends of air temperature anomalies in the Arctic faithfully reproduce both the long-term components of the DG_{3L} index and, in most cases, its short-term decreases or increases. In particular periods of increases and decreases (rises and falls in the DG_{3L} index and air temperature anomalies in the Arctic show concordant trends and statistically significant correlations between both the positive and negative swings are observed. This means that correlations between DG_{3L} and air temperature anomalies in the Arctic over the whole 130 years long period are not exclusively the result of trends in either series. Such a finding sets the questions of the genesis of climate changes in the Arctic, and whether intra-system or extra-system mechanisms determine the climate variability there.

[22] North Atlantic SST averages, unsmoothed and undetrended, from the NOAA ERSST V2 SST, interpolated to a 5x5 grid. (http://www.esrl.noaa.gov/psd/data/correlation/amon.us.long.mean.data).

[23] Unsmoothed, long (http://www.esrl.noaa.gov/psd/data/correlation/amon.us.long.data).